PB-230 373

POLLUTANTS FROM METHANE FUELED GAS TURBINE COMBUSTION

Pradip G. Parikh, et al

California University
Berkeley, California

January 1971

DISTRIBUTED BY:

NTIS

National Technical Information Service
U. S. DEPARTMENT OF COMMERCE
5285 Port Royal Road, Springfield Va. 22151

AP 7.1-55

PB 230 373

POLLUTANTS FROM METHANE FUELED GAS TURBINE COMBUSTION

Pradip G. Parikh
Robert F. Sawyer
A. L. London

University of California
College of Engineering
Report No. TS-70-15

Grant PHS AP 00385

January 1971

COLLEGE OF ENGINEERING

UNIVERSITY OF CALIFORNIA, Berkeley

Reproduced by
NATIONAL TECHNICAL
INFORMATION SERVICE
U S Department of Commerce
Springfield VA 22151

98

UNITED ST... GOVERNMENT PROPERTY
This book is the prop... the United States Go... Air Pollution Control

POLLUTANTS FROM METHANE FUELED GAS TURBINE COMBUSTION

Pradip G. Parikh[1]
Robert F. Sawyer[2]
A. L. London[3]

Property of:
Air Pollution Control Office
Reference Library

[1]Graduate student, Dept. of Aeronautics & Astronautics, Stanford University.

[2]Associate Professor, Thermal Systems Division, Mechanical Engr. Dept., University of California, Berkeley.

[3]Professor, Thermosciences Division, Mechanical Engineering Dept., Stanford University.

ABSTRACT

The air pollution characteristics of a model gas turbine type combustor using methane as fuel were studied in this investigation. Detailed information regarding gas compositions at various locations within the combustor was obtained by analysis of gas samples withdrawn by a water cooled probe. Direct measurement of temperature within the combustor was carried out by means of a thermocouple. The essential differences between air pollution characteristics of gaseous and liquid fuels used in the combustor were investigated. Performances of two nozzles employing two different gas injection velocities were compared. Influence of overall equivalence ratio on hydrocarbons and CO emissions was evaluated. Information regarding air flow distribution in the combustor was obtained from axial distribution of averaged local equivalence ratio. An estimate of the characteristic time of combustor flow processes was obtained for a comparison with characteristic time of NO formation by Zel'dovich mechanism in adiabatic methane - air combustion. Significantly low values not only of CO and hydrocarbons but also of NO concentrations were obtained with the use of methane.

ACKNOWLEDGEMENTS

This research was conducted in the Thermal Systems Division of Mechanical Engineering Department at the University of California at Berkeley under the auspices of the Graduate Student Exchange Program between Stanford University and University of California at Berkeley. The financial support for this work was provided by the National Air Pollution Control Administration under Grant AP-00385 and the Office of Naval Research under Contract NONR 225(91).

Messrs. D. Giovanni, N. Moussa, M. McElroy and S. G. Prakash assisted in the collection of data. Their help is gratefully acknowledged.

Finally, thanks are also due to the Hesse Hall Laboratory personnel of U.C. Berkeley for their assistance in handling and maintenance of equipment.

TABLE OF CONTENTS

	Page
ABSTRACT	iii
ACKNOWLEDGEMENTS	iv
TABLE OF CONTENTS	v
LIST OF FIGURES	vii
LIST OF TABLES	x
NOMENCLATURE	xi
1. INTRODUCTION	1
1.1 The Spark Ignition I. C. Engine vs Gas Turbine	1
1.2 Contribution of Gas Turbine to Air Pollution	11
1.3 Air Pollution Characteristics of Gas Turbine Engines	11
1.4 Objectives of Experimental Investigation	14
2. EXPERIMENTAL INVESTIGATION	16
2.1 Combustor Test Facility	16
2.2 Gas Sampling and Temperature Measurement Techniques	23
2.3 Gas Analysis Instrumentation	27
2.4 Test Procedure	30
2.5 Test Results	34
3. DISCUSSION OF RESULTS	36
3.1 Axial Distribution of Averaged CO_2, CO and Hydrocarbon Concentrations	36
3.2 Axial Distribution of Averaged Local Equivalence Ratio and Airflow	49
3.3 Problem of NO Formation	56

Page

4. SUMMARY AND CONCLUSIONS. 72

REFERENCES 74

APPENDIX A. Conversions for Emission Data 77

APPENDIX B. Calculation of Local Equivalence Ratio and Oxygen Mol Fraction 79

APPENDIX C. Kinetics of NO Formation. 84

LIST OF FIGURES

Figure		Page
1	Contribution of Gasoline Powered Motor Vehicles to the Total Air Pollution in U.S.	2
2	California Air Resources Board Emission Standards	4
3	Effect of Equivalence Ratio on HC's and CO Emissions From Aircraft Gas Turbines	12
4	Details of Liner Hole Location	17
5	Details of Gas Injector	18
6	The Combustor Test Facility	20
7	Sampling Probe and Thermocouple	22
8	Locating Device	24
9	Sample Cooling System and Analyzer Train	29
10	Probe Trace and Sampling Locations Within the Combustor	31
11	Axial Distribution of Averaged CO_2, CO and Hydrocarbons - Low Velocity Nozzle	38
12	Axial Distribution of Averaged CO and Hydrocarbons - High Velocity Nozzle	39
13	Axial Distribution of Averaged CO_2	40
14	Axial Distribution of Averaged CO and Hydrocarbons $\varphi_o = 0.27$	42
15	Axial Distribution of Averaged and Centerline CO and Hydrocarbons - $\varphi_o = 0.27$	44
16	Axial Distribution of Averaged CO and Hydrocarbons $\varphi_o = 0.20$	45
17	Comparison of Axial Distribution of Averaged CO and Hydrocarbons for Heptane and Methane	48
18	Axial Distribution of Averaged Local Equivalence Ratio and O_2 - $\varphi_o = 0.20$, H.V.N.	50

Figure		Page
19	Axial Distribution of Averaged Local Equivalence Ratio and $O_2 - \varphi_o = 0.20$, L.V.N.	50
20	Axial Distribution of Averaged Local Equivalence Ratio and $O_2 - \varphi_o = 0.27$, H.V.N.	50
21	Axial Distribution of Averaged Local Equivalence Ratio and $O_2 - \varphi_o = 0.27$, L.V.N.	50
22	Axial Distribution of Averaged Local Equivalence Ratio	52
23	Radial Equivalence Ratio Distribution at 3" Axial Station - L.V.N.	52
24	Radial Equivalence Ratio Distribution at 3" Axial Station - $\varphi_o = 0.27$	52
25	Axial Airflow Distribution	54
26	Radial Distribution of NO Concentration at 2" Axial Station - $\varphi_o = 0.27$, L.V.N.	57
27	Radial Distribution of NO Concentration and Temperature at 2½" Axial Station - $\varphi_o = 0.27$, L.V.N.	57
28	Radial Distribution of NO Concentration and Temperature at 3" Axial Station $\varphi_o = 0.27$, L.V.N.	57
29	Radial Distribution of NO Concentration at 3½" Axial Station - $\varphi_o = 0.27$, L.V.N.	57
30	Radial Distribution of NO Concentration and Temperature at 4" Axial Station - $\varphi_o = 0.27$, L.V.N.	58
31	Radial Distribution of NO Concentration at 5" Axial Station $\varphi_o = 0.27$, L.V.N.	58
32	Radial Distribution of NO Concentration at 7" Axial Station $\varphi_o = 0.27$, L.V.N.	58
33	Radial Distribution of NO Concentration and Temperature at 8" Axial Station. $\varphi_o = 0.27$, L.V.N.	58

Figure		Page
34	Radial Distribution of NO Concentration and Temperature at 12" Axial Station φ_o = 0.27, L.V.N.	59
35	Radial Distribution of NO Concentration at Various Axial Stations - φ_o = 0.27, L.V.N., Negative Rotation of Probe	59
36	Axial Distribution of Averaged NO Concentrations and Temperature - φ_o = 0.27, L.V.N.	60
37	Equilibrium NO Concentration and Flame Temperature in Adiabatic Methane-Air Combustion-$T_{initial}$ = 298°K p = 1 ata	62
38	Axial Distribution of Averaged Density and Velocity (Calculated From Measured Temperatures) - φ_o = 0.27, L.V.N.	64
39	Time Histories of Averaged Local Equivalence Ratio, Temperature and NO Concentrations - φ_o = 0.27, L.V.N.	65
40	Non-Equilibrium NO Formation in the Products of Adiabatic Combustion of Methane and Air - $T_{initial}$ = 298°K, p = 1 ata	66
41	Radial Distributions of NO and Local Equivalence Ratio at 3" Axial Station - φ_o = 0.27, L.V.N. . .	68
42	Comparison of Averaged Axial NO Distribution for Methane and Heptane	70

LIST OF TABLES

Table		Page
I	California Air Resources Board Emission Standards	3
II	Emission Data for Vehicular Gas Turbines	6
III	Emission Data for Aircraft Gas Turbine Engines	12

NOMENCLATURE

LIST OF SYMBOLS

$\dot{m}_{f,\ act}$ = actual mass flow rate of fuel (methane)

$\dot{m}_{f,\ std}$ = mass flow rate of methane given by standard rotameter calibration curve corresponding to observed float position

T = temperature °K

p = pressure (psia or ata)

x_a = mass of air passing through a given axial station expressed as a function of total air flow

V_{ave} = average axial velocity at a station

Y_{ppm} = mole fraction of species Y in parts per million

X_y, N_y = mole fraction of species Y

$\hat{M}_y$ = molecular weight of species y

$\hat{M}_{exh}$ = average molecular weight of exhaust

$(A/F)_s$ = stoichiometric air/fuel ratio

$(A/F)_{actual}$ = actual air/fuel ratio

φ = equivalence ratio $\triangleq \dfrac{(Fuel/Air)_{actual}}{(Fuel/Air)_{stoichiometric}}$

φ_o = overall equivalence ratio

φ_L^{ave} = average local equivalence ratio

EI_y = emission index of species Y

$= \dfrac{\text{mass flow rate of Y in exhaust}}{\text{mass flow rate of fuel}} \times 10^3$

F_M = mass of fuel consumed per mile

ν = stoichiometric coefficient

k_{1f} = forward rate constant for reaction (1)

k_{1b} = backward rate constant for reaction (1)

$\hat{R}$ = universal gas constant

1. INTRODUCTION

1.1 The Spark Ignition I. C. Engine vs Gas Turbine

The principal single cause of the deterioration of air quality standards in urban areas throughout the world is the familiar automobile engine. It maintains this position due both to the sheer weight of numbers in thickly populated urban areas and the poor quality of its exhaust from air pollution viewpoint. Figure 1 [1]* provides an estimate of the relative contribution of motor vehicles to the air pollution problem in the United States.

The pollutants of major concern from motor vehicles are carbon monoxide, a toxic gas in itself, hydrocarbons and oxides of nitrogen, the latter two having been identified as the constituents of photochemical smog. In an effort to reduce the motor vehicle air pollution, the federal and state governments have established a program of emission standards. The California Air Resources Board (CARB), formerly the California Motor Vehicle Pollution Control Board, emission standards through the year 1980 are presented in Table I and the increasing stringency of these standards is depicted in Fig. 2.

Both the government and the industry have directed considerable effort toward improving the quality of exhaust from the vehicles of transportation. The largest proportion of the latter effort consists in controlling the emissions of CO , NO_x and hydrocarbons from the four stroke cycle, spark ignition automobile engine. A summary of the current and proposed technical approaches to control emissions from the

* Numbers in square parentheses indicate references.

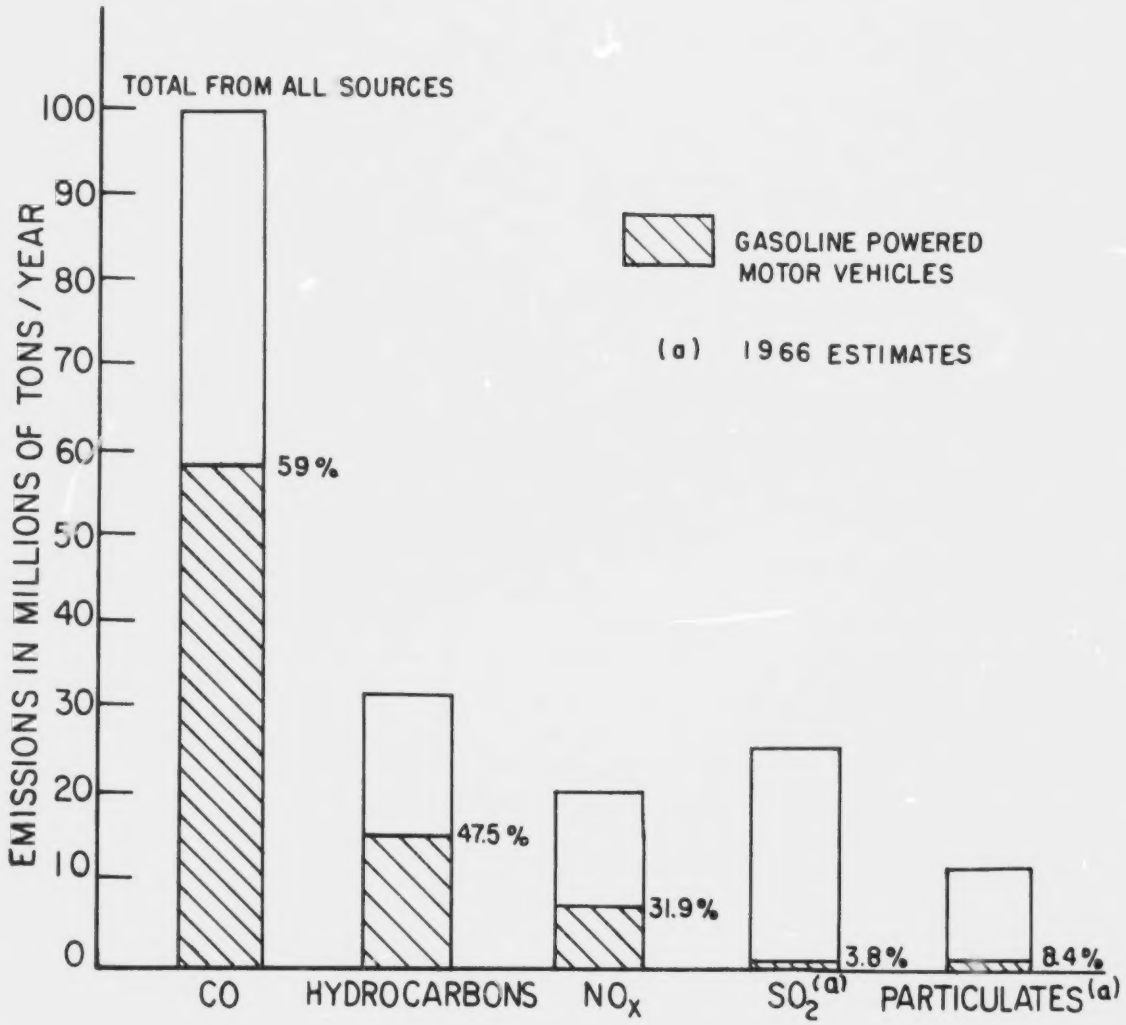

Figure 1. Contribution of Gasoline Powered Motor Vehicles to the Total Air Pollution in U.S.

TABLE I

CALIFORNIA AIR RESOURCES BOARD EMISSION STANDARDS

[H.E.W. 7 Cycle Cold Start Emission Test]

	MOTOR VEHICLE EMISSION STANDARDS GMS/MILE			
YEAR	HC'S	NO_x	CO	
No Control	11.0	~4.0	80	
1968	3.4	-	34	
1970	2.2	-	23	
1971	2.2	4.0	23	
1972	1.5	3.0	23	
1974	1.5	1.3	23	
1975	0.5	1.0	12	PROPOSED
1980	0.25	0.4	4.7	

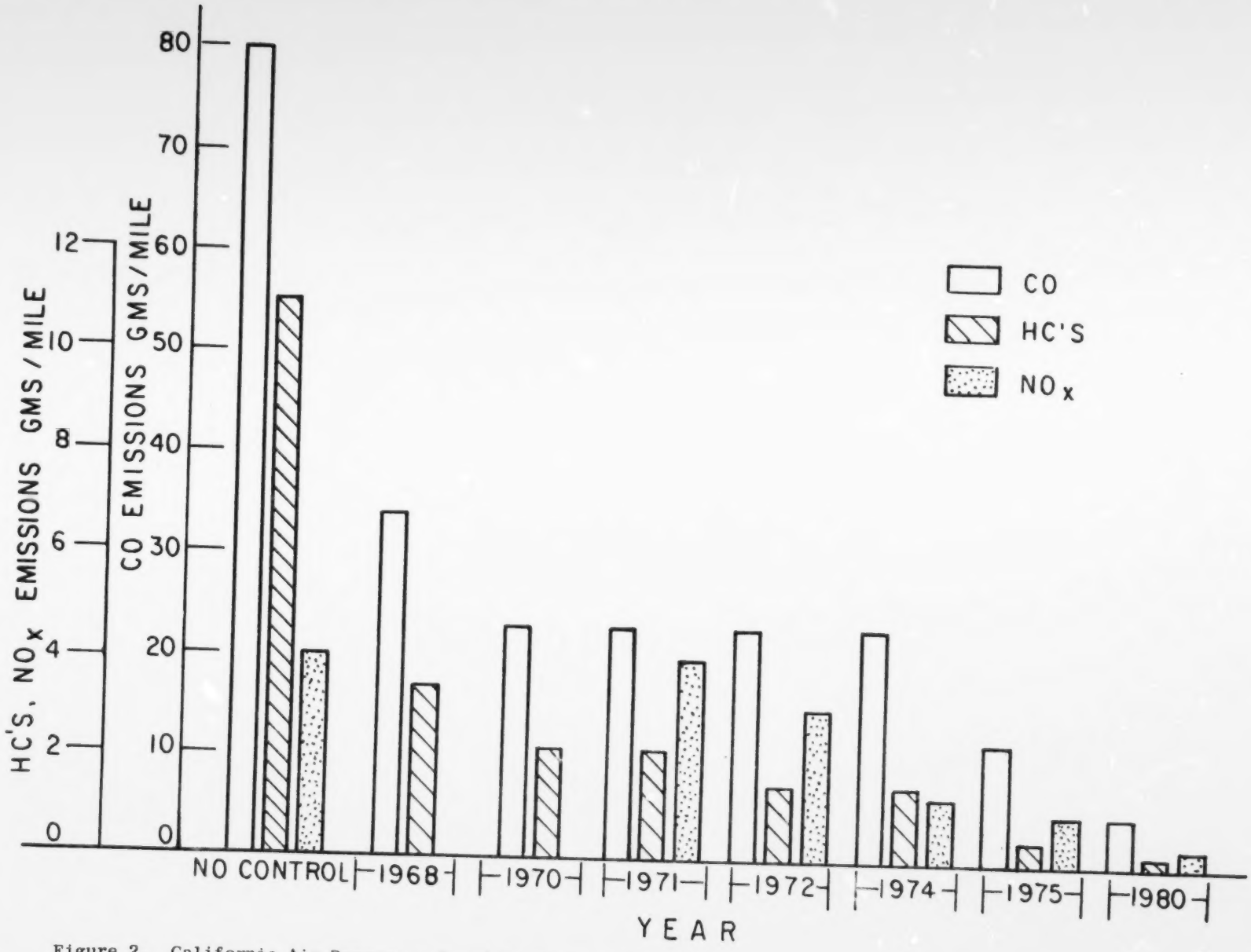

Figure 2. California Air Resources Board Emission Standards.

latter engine is presented in [1]. In principle, emissions from the spark ignition I. C. engine may be reduced either by reducing their production in the engine, or by treatment of the exhaust before discharge to the atmosphere or by a combination of these two approaches. To meet the 1972 CARB emission standards, engine modifications alone will suffice, however, to achieve the emission targets for 1975 and beyond exhaust gas treatment will be needed [1]. Not only are the proposed exhaust treatment devices to meet the emission standards of 1975 and beyond expensive, they also show poor potential of development [1]. It appears, therefore, that in the face of the increasingly high cost of the auxilliary control devices to meet restrictive emission standards of the future, the spark ignition I. C. engine will lose much of its present economical advantages and will consequently be subjected to increasing competition from other power plants of low air pollution potential.

One of the most promising alternatives to the spark ignition I. C. engine is the gas turbine, already highly developed in its application as an aircraft power plant. In view of its outstanding success in the field of aviation, the feasibility of its application to the propulsion of ground vehicles has been explored over the last two decades and successful regenerative vehicular gas turbines have been developed. Little consideration was given, until recently, to low air pollutant emission requirement in the design of their combustion systems. In spite of this neglect, however, measurements of its exhaust gas composition have shown it to possess superior emission characteristics over those of the spark ignition I. C. engine. This particular

TABLE II

EMISSION DATA FOR VEHICULAR GAS TURBINES

ENGINE	H.E.W. COMPOSITE EMISSIONS GMS/MILE			REF.
	HC'S	NO_x	CO	
Chrysler 130 H.P. Vehicular Gas Turbine	0•91	1•86	7•03	3
GM GT-309 280 H.P. Regenerative Vehicular Gas Turbine with Standard Burner	0•3	3•75	2•25	2
GM Hypothetical Gas Turbine Car Simulation With a Modified Burner for a 200 H.P. Engine	0•24	2•0	4•7	Fig.23 of 21
1971 CARB* Emission Standards	2•2	4	23	1
1980 Proposed CARB* Emission Standards	0•25	0•4	4•7	1

* California Air Resources Board

feature of the gas turbine adds the greatest incentive of its use in ground vehicle propulsion. A comparison between emissions from a 1971 spark ignition I. C. engine and vehicular gas turbines is presented in Table II.

In order to investigate this superiority of gas turbine exhaust emissions of CO , NO_x and hydrocarbons over those of the spark ignition I. C. engine, it is necessary to study the nature of combustion process in the two engine types. The four major distinctions between the two types are:

(a) While the range of equivalence ratios[1] used in a spark ignition I. C. engine is near unity over all operating conditions, it varies in the range 0.05 to 0.3 for the gas turbine.

(b) The combustion in a spark ignition I. C. engine takes place nearly at constant volume while that in a gas turbine is essentially at constant pressure.

(c) Combustion in a spark ignition I. C. engine is intermittent, while that in a gas turbine is continuous.

(d) In a spark ignition I. C. engine, combustion takes place as a flame propagating in a homogeneous mixture of air and vaporized fuel while the gas composition in the combustion zone of a gas turbine is necessarily inhomogeneous. Local fuel rich zones exist around vaporizing fuel droplets.

---

1 The equivalence ratio φ is defined as

$$\varphi \triangleq \frac{[\text{Fuel/Air}]_{\text{Actual}}}{[\text{Fuel/Air}]_{\text{Stoichiometric}}}$$

The consequences of these four distinctions in the two types of combustion process and their effects on the emission characteristics will now be discussed.

(a) Some desirable operating characteristics associated with fuel-air mixtures richer than the stoichiometric have traditionally favored the employment of such mixtures in the spark ignition I. C. engines. Equilibrium considerations show CO to be a species present in significant proportions in the products of combustion of rich mixtures [4]. Both kinetic considerations of the expansion process and spectroscopic studies further show that no significant oxidation of CO occurs during the expansion process and the concentrations of CO appearing in the exhaust conform closely to a frozen expansion [4,5,6].

On the other hand, the abundance of excess air available in the dilution zone of a gas turbine combustor together with a sufficiently high temperature level allows a more complete combustion of the fuel and this is the primary reason why exhaust emissions of hydrocarbons and CO are so low relative to the spark ignition I. C. engine.

(b) It has been shown that the equilibrium concentration of NO is a strong function of temperature and that the rate of formation of NO is strongly dependent on temperature and shows a positive dependence on the square root of pressure [7]. The constant volume combustion of fuel-air mixtures in a piston engine results in temperatures in excess of 3000° K and peak pressures of the order

of 100 atm.[8]. Both pressure and temperature in an aircraft gas turbine combustor are lower - in the range 10-20 atm and 2500° K. Temperatures in a regenerative vehicular gas turbine approach those attained in piston engines due to high degree of preheat, but the pressures are low - generally less than 5 atm. Design solutions, moreover, appear feasible to lower the maximum temperature by leaning out the primary zone [21]. Thus while the relatively fixed conditions in a piston engine favor a high formation rate and high equilibrium concentrations of NO , the designer has a considerable control of the combustion variables in the gas turbine engine.

(c) The intermittency of the combustion process is an inherent disadvantage of piston engines as far as hydrocarbon emissions are concerned. A consequence of the intermittency of the combustion process is the presence of cool walls which are responsible for the quenching of the flame at the boundaries of the bulk gas. This quenched zone is the seat of production of unburned hydrocarbons. Ironically, one of the methods employed to suppress knock in spark ignition I. C. engines has been to keep the end gas cool by presenting large surface area [8]. Hence the new requirement of lower surface to volume ratios of the combustion chamber to reduce unburned hydrocarbons appears contradictory to the requirements for suppression of knock.

A further consequence of the intermittent combustion together with finite flame propagation rates in spark ignition I. C. engines

is the presence of a temperature gradient amounting to as much as 400°K. The burnt charge in the immediate vicinity of the spark plug attains temperatures higher than the bulk temperature [8]. The presence of local high temperature regions thus further adds to NO production.

Continuous combustion of the gas turbine preserves the liner walls near the injector at sufficiently high temperatures, so that practically no production of hydrocarbons results from surface quenching.

(d) The last distinction between the combustion processes of gas turbine and spark ignition I. C. engine is closely related to smoke emissions. The premixed and prevaporized mixture of spark ignition I. C. engine does not lead to formation of carbon particles, while the presence of fuel rich zones in the diffusion flame of a liquid fuel spray presents problem of smoke emissions from gas turbine combustors.

Of all the pollutants emitted from aircraft gas turbines, smoke has received greatest attention up to the present time [9,10,11] and visible smoke emissions from the new aircraft gas turbines have been practically eliminated by combustor design changes. The problem of smoke as well as aldehydes and aerosol formation in gas turbine combustors is not investigated in this work.

1.2 The Contribution of Gas Turbine to Air Pollution

The principal application of the gas turbine at the present time is as an aircraft power plant. Consequently, the contribution of gas turbine to air pollution mainly comprises the emissions from aircraft jet engines. In view of characteristically low emission feature of the gas turbine together with negligible operation of jet aircraft relative to motor vehicle operation over urban areas, the contribution of aircraft jet engines to the total community-wide air pollution burden is negligible. However, as several studies have concluded, the impact of jet engine exhaust emissions is of localized nature and in the vicinity of air terminals their contribution to the air pollution problem becomes comparable to that from other sources [12,13,14]. Also, the relative contribution of jet aircraft to the total air pollution burden cannot be counted upon to remain small in view of the projected growth of air transportation, advent of high capacity bypass engines and control of emissions from other sources.

The usage of gas turbines as central station power plants for electrical energy generation is expected to increase significantly. These considerations as well as the application of gas turbines in ground vehicle propulsion, expected to begin in mid 1971 have stimulated greatly the study to better understand the processes governing the production of pollutants in gas turbine combustors.

1.3 Air Pollution Characteristics of Gas Turbine Engines

As a first step toward the understanding of gas turbine emissions, numerous studies [12,13,15,16] concerning detailed measurements of the

TABLE III

EMISSION DATA FROM AIRCRAFT GAS TURBINE ENGINES

ENGINE	MODE OF OPERATION	EQ. RATIO Φ	POLLUTANT EMISSION INDEX LBS/LB OF FUEL CONSUMED x 10^3				REFERENCE
			CO	NO	HC'S	PARTICULATES	
J-57 (Turbojet)	Take Off	0.212	2·11	6·5	0·145	14	12,17
	Cruise	0.159	5·02	5·84	0·20	7	
	Idle	0.077	23·5	3·82	11·8	10	
TF-33 (Turbofan)	Take Off	0.197	0·35	3·32	0·28	1.9	12
	Cruise	0.176	2·4	1·97	1·76	2·02	
	Idle	0.0964	28·1	2·6	43·2	2·4	
JT-8D (Turbofan)	Take Off	0.24	1·4	5·8	2·5		15
	Cruise	0.20	3·2	6·3	3·5		
	Idle	0.13	34	2·7	11·4		

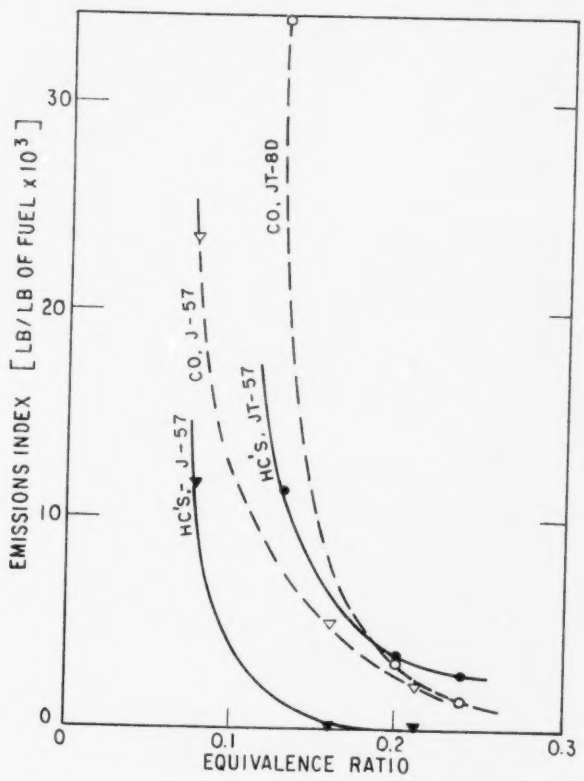

Figure 3. Effect of Equivalence Ratio on HC's and CO Emissions From Aircraft Gas Turbines

composition of exhaust from industrial and aircraft gas turbines have been conducted following the pioneering work of George and Burlin [17]. Some of the results of such studies are presented in Table III. (Relations between the Emission Index measure used here and mol fractions and gms/mile measures are derived in Appendix A.) The hydrocarbon and CO data for two engines are plotted against the equivalence ratio in Fig. (3). All measurements of the composition of exhaust from gas turbines have shown that levels of CO , NO and hydrocarbons do not correspond to those predicted for chemical equilibrium at exhaust conditions [15,19]. Further, in contrast to the equilibrium prediction, the concentrations of CO and hydrocarbons are found in Fig. 3 to decrease with increasing equivalence ratio. The causes responsible for these trends are traceable to the fundamental processes occurring in the combustor. It has also become evident that factors which could reduce CO and hydrocarbon emissions from gas turbines are precisely those that tend to increase the NO emission levels. This trend is apparent from Table III.

One of the most direct methods of studying the fundamental processes governing production of pollutants in a gas turbine combustor is the measurement of gas compositions and temperature at various locations within the combustor. Such a detailed specification of conditions within the combustor lends insight into the mechanism of pollutant formation.

In a previous investigation [18], detailed information regarding gas composition within a model gas turbine combustor was obtained using liquid heptane as fuel. Little information exists on the use of gaseous fuels for gas turbine applications. The use of natural gas (liquefied

or compressed) for conventional spark ignition I. C. engines is being investigated and results have indicated substantial reduction in pollutant emissions [20]. The success of gaseous fuels was further demonstrated by the "Clean Air Car Race" in August 1970. Of the seven cars that bettered 1975 Federal emission standards at the end of the race, six were gaseous fueled and one fueled by alcohol. Moreover, four of these six gaseous fueled cars showed lower emissions than the alcohol car [29]. Natural gas is being used in many stationary power plant installations for electrical energy generation and natural gas line compressor stations. The present investigation was initiated to determine the air pollution characteristics of a gaseous fuel used in a gas turbine combustor. It was hoped that the information obtained would also find applicability to gas turbines employing prevaporized fuel injection systems. For reasons of its large proportion in composition of natural gas, availability and ease of analysis, methane was selected as the fuel.

1.4 The Objectives of the Experimental Investigation

The objectives of the present experimental investigation are:

(a) To determine the gas compositions within a model gas turbine type combustor, burning methane, by withdrawing gas samples at various locations by means of a water cooled probe and thereby to follow, in detail, the processes of formation and/or depletion of certain chemical species important from an air pollution viewpoint.

(b) To compare the air pollution characteristics of a gaseous

fuel (methane) with those of a liquid fuel (heptane) used in a previous investigation [18] in the model combustor.

(c) To study the effect of overall equivalence ratio on the air pollution characteristics of the model combustor.

(d) To carry out a direct measurement of temperature at various locations within the combustor by means of a thermocouple probe.

(e) To compare the performance of two gas nozzles employing different injection velocities.

2. EXPERIMENTAL INVESTIGATION

2.1 The Combustor Test Facility

The combustor assembly consists of a 3" O.D. by 14" long inconel liner enclosed in a 3-3/4" I.D. pyrex tube. The liner contains 80 3/16" dia. holes drilled in ten equispaced circumferential rows with 8 holes per row. The hemispherical dome of the liner contains 12 radial slots and a central 5/8" dia. hole for introduction of the fuel nozzle. The details of the hole locations are shown in Fig. 4.

Air is supplied to the combustor head by three air hoses symmetrically spaced on the head and supplying air radially. After thorough mixing in the head the air flows axially into the pyrex tube and thence into the liner through the slots and holes. Ignition of the fuel is achieved by means of a spark created between two tungsten electrodes approximately 1" downstream from the nozzle and near the liner wall. The transparent pyrex tube permitted visual observation of the flame, spark discharge and nozzle location through the holes in the inconel liner. The nozzle assembly was fairly accessible for occasional inspection and nozzle replacement, with limited freedom for variation in axial location and orientation of the nozzle.

Due to lack of available information on gas nozzles for gas turbine applications and for expediency, a simple configuration with 12 holes drilled at an inclination of 50° to the centerline was adopted (Fig. 5). Two stainless steel nozzles were machined with hole diameters of 1/64" and 1/32" respectively, designed to give 1100 ft/sec and 300 ft/sec gas velocities for a methane flow rate of approximately 4 lbm/hr.

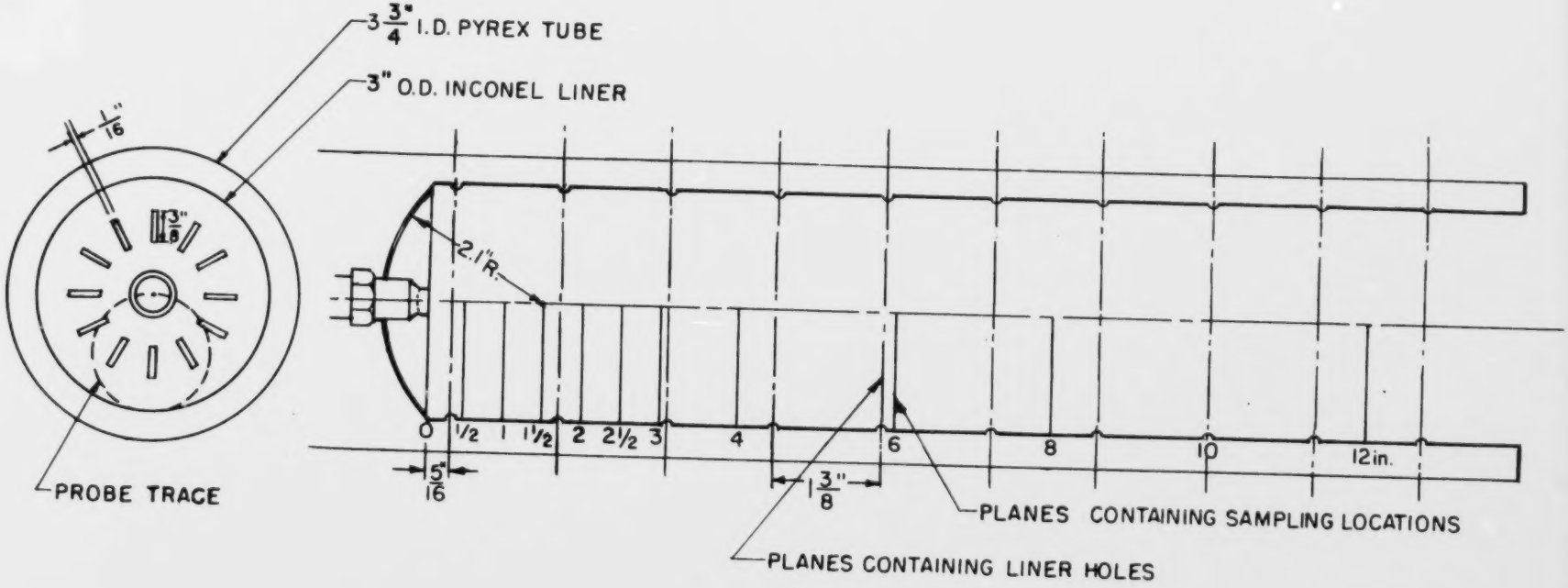

Figure 4. Details of Liner Hole Location

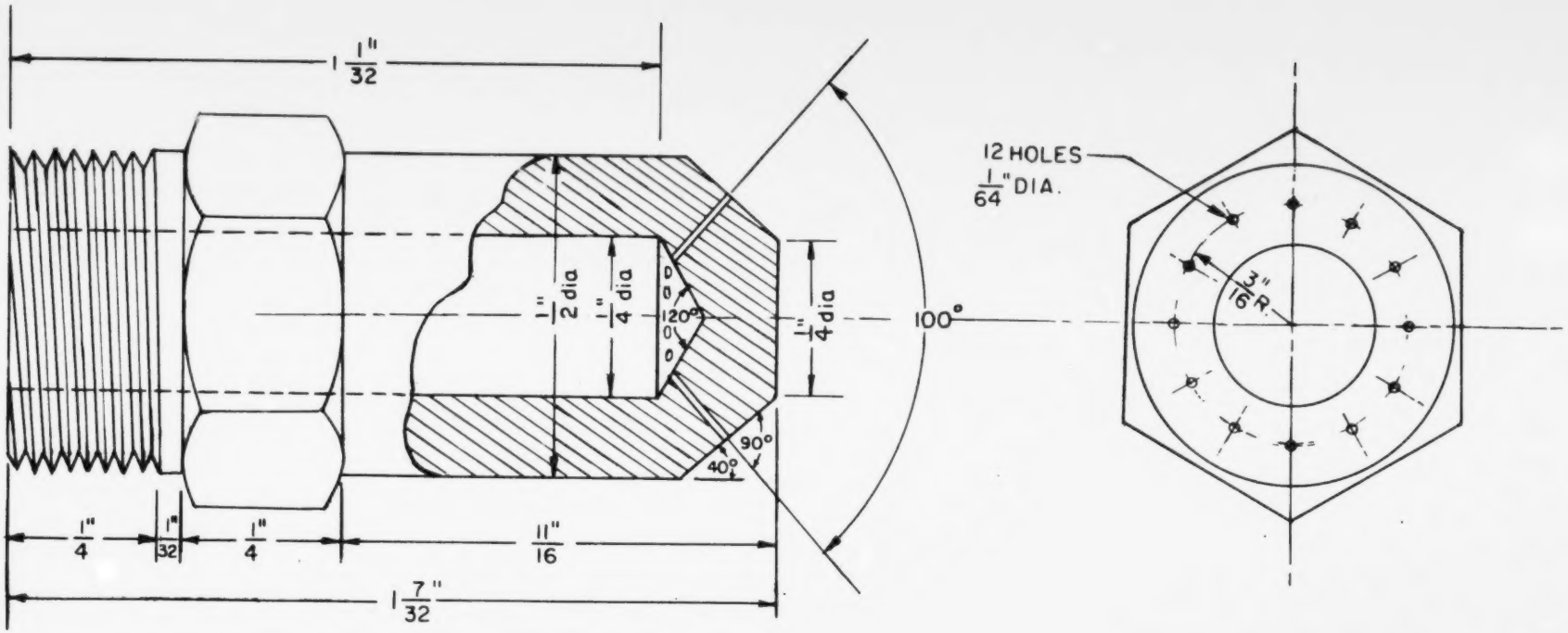

SPECIFICATIONS:

(1) METHANE FLOW RATE: 5 lbm/hr ≐ 2 cfm AT 70°F, 1 ata
(2) SUPPLY PRESSURE: 3 ata
(3) CHAMBER PRESSURE: 1.5 ata
(4) JET VELOCITY: ≈ 1300 ft/sec

SCALE: 4:1
MATERIAL: STAINLESS STEEL

Figure 5. Details of Gas Injector

(Incidentally, this gave, assuming a complete combustion of fuel, a heat release rate of approximately 10^6 BTU/(ft^3-hr-atm) for the given dimensions of the combustor and 1.2 atm operating pressure. This is comparable to heat release rates of 0.7 to 3 x 10^6 BTU/(ft^3-hr-atm) for industrial gas turbines and is less than 3 to 11 x 10^6 BTU/(ft^3-hr-atm) for aircraft gas turbines [22].) It was hoped that this nozzle would provide a fuel distribution similar to that provided by the liquid fuel injector employed in a previous investigation [18].

The exhaust gases from the combustor were passed through an orifice constriction at the end of the liner to maintain the pressure in the combustor slightly higher than atmospheric. Immediately upon their exit from the combustor, the exhaust gases were cooled by means of water sprays. The water was supplied at a constant rate from a pressurized tank. The temperature of the exhaust after cooling by water sprays was measured by a Chromel-Alumel thermocouple and was continuously monitored on a strip chart recorder. A constant reading on the recorder indicated attainment of steady state in the combustor. Further downstream in the exhaust line a sampling tap was provided to extract exhaust sample for determination of overall equivalence ratio. It was expected that exhaust gases had attained homogeneity in chemical composition at this sampling tap after passing through 3 elbows in the exhaust line (Fig. 6).

Air at 52 psig was available from laboratory supply for the combustor test rig. The airflow rate was metered by an orifice meter. The knowledge of the airflow rate was fairly accurate as was later found from the calculations of overall equivalence ratios.

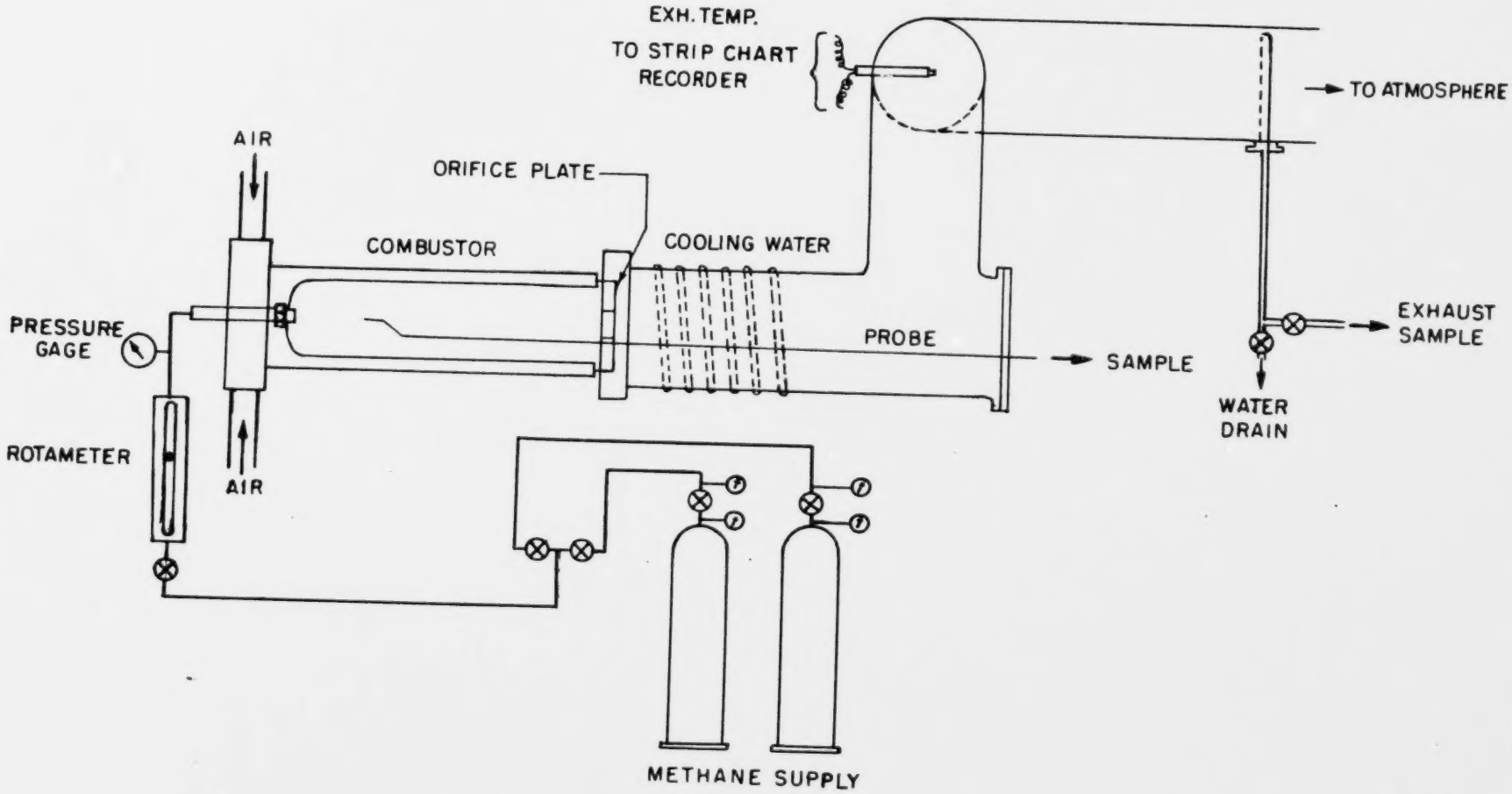

Figure 6. The Combustor Test Facility

The fuel, commercial grade methane was supplied in 350 std. cu. ft. capacity cylinders by Baker Chemical Co., Los Angeles, California. With a methane flow rate of approximately 100 std. cu. ft. per hour, it was necessary to connect two cylinders to the fuel supply line as shown in Fig. 6. This arrangement made possible the replacement of empty cylinders while supplying methane continuously for long periods of test runs. The methane flow rate was metered by a rotameter and a pressure gauge, both being situated a short length of 1/4" copper tubing upstream of the fuel nozzle. The rotameter calibration curve supplied by the manufacturer was for standard temperature and pressure. To correct for higher methane pressure, the following formula was used:

(Ref. Handbook of Flow Meters ASME)

$$\dot{m}_f act = \dot{m}_f std \times \frac{\sqrt{p/p_{std}}}{\sqrt{T/T_{std}}}$$

where,

$\dot{m}_f act$ = actual mass flow rate of methane

$\dot{m}_f std$ = mass flow rate of methane given by standard calibration curve corresponding to observed rotameter reading

T,p = actual temperature ($^{\circ}K$) and pressure

and

T_{std}, p_{std} = standard temperature ($^{\circ}K$) and pressure on calibration chart

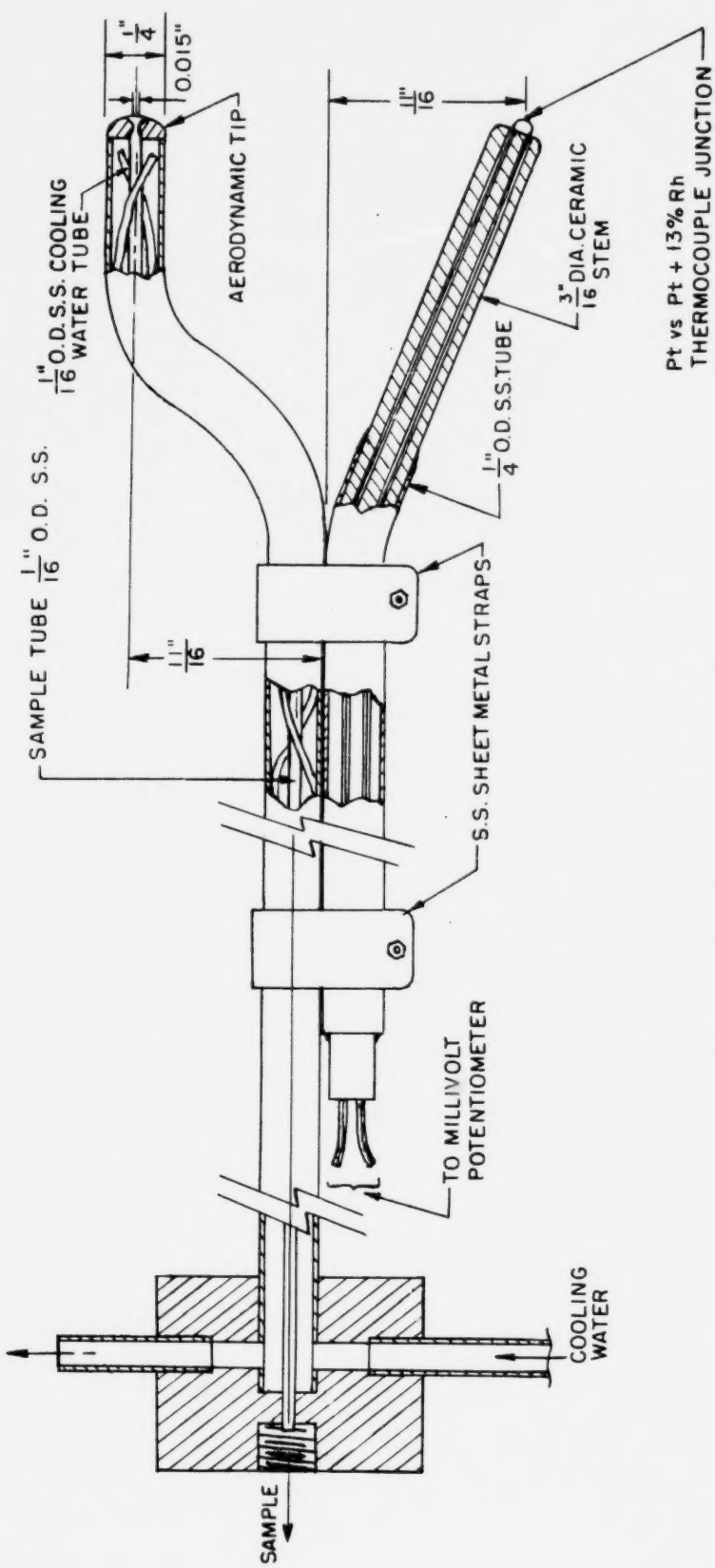

Figure 7. Sampling Probe and Thermocouple

This simple relation did not provide a sufficiently accurate correction for pressure, however, no error was introduced in the determination of overall equivalence ratios, since these were calculated from accurately measured exhaust compositions.

2.2 Gas Sampling and Temperature Measurement Techniques

As mentioned earlier, the determination of local gas compositions by analysis of the samples withdrawn at various locations is the principal objective of this investigation. The selection of the sampling locations was dictated by an intuitive assumption of an axisymmetric flow pattern within the combustor. For the purpose of studying the formation and/or depletion of certain chemical species as the reacting flow progresses downstream, it was decided to take samples at planes normal to the axis of the combustor and at various distances from the fuel nozzle. In order to study the radial gradients in each of these planes it was necessary to take samples at varying distances from the centerline in that plane. And in order to verify the axisymmetric flow assumption, it was necessary to take samples along different radial lines, at same distance from the centerline in a normal plane. It was also desirable to measure temperature at the points where samples were extracted. In addition, the probe must accomplish a sufficiently rapid quenching of the sample in order to get a true gas composition at a point and must maintain its structural integrity in the high temperature and corrosive combustion environment.

Most of these requirements were satisfied by the probe used in an earlier investigation [18]. The stainless steel probe with a 11/16"

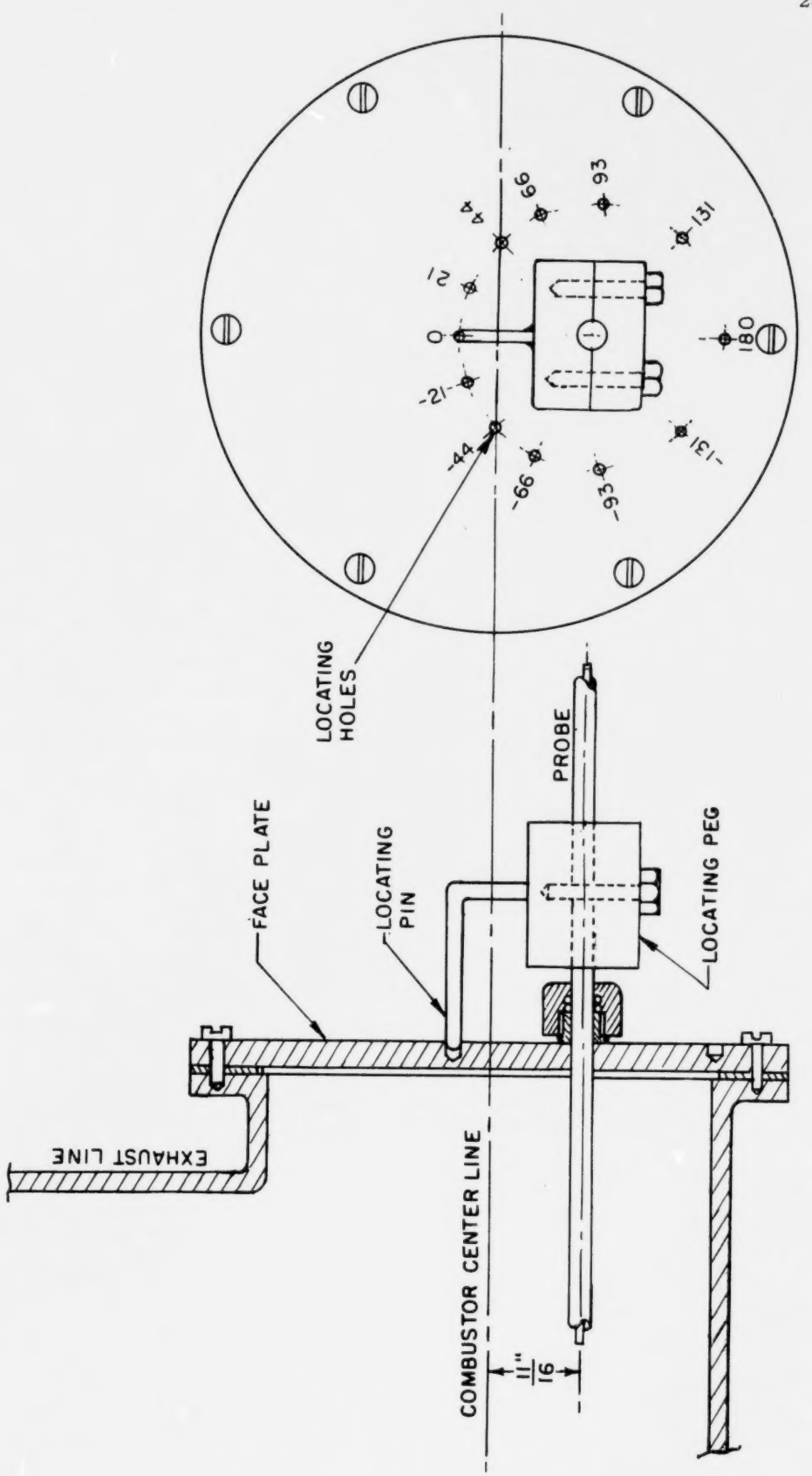

Figure 8. Locating Device

offset tip was introduced through an eccentrically drilled hole in a face plate which was mounted at the first elbow in the exhaust line. The packing in the face plate provided a rigid but sliding support to the probe. A second support was provided at the combustor exhaust section by passing the probe through a hole in the split orifice plate. Due to the eccentric mounting of the probe, the probe tip traces a circle in the lower half of the combustor with the diameter of the trace circle equal to the radius of the liner as shown in Fig. (10). Thus, by rotating the probe it is possible to cover points in a plane at various distances and directions from the centerline and by sliding the probe back and forth it is possible to cover all planes at distances up to 12" from the fuel nozzle.

The requirement of temperature measurement at locations of sample withdrawal was accomplished by mounting a Pt vs Pt + 13% Rh thermocouple on a ceramic piece diametrically opposite to the sampling probe tip as shown in Fig. (7). Thus, it was made possible to take temperature measurements at points coinciding with sampling locations simply by rotating the probe through 180°.

Dead end holes were drilled in the probe supporting face plate representing angles of probe rotation corresponding to radial distances of 0, 1/4, 1/2, 3/4, 1, 1-1/4 and 1-1/2 inches from the centerline. A locating peg which could be fastened to the probe was inserted in a locating hole of the face plate to prevent inadvertent rotation of the probe while the sample was being withdrawn (Fig. 8).

The cooling water to the probe was supplied at 100 psig by three 1/16" dia.S.S. tubes helically wrapped around the sampling tube, also

1/16" dia. The tubes discharge water at the probe tip from where it flows back through the annular passage between the sample tube and the outer 1/4" dia. S.S. tube. The water had to be filtered before its flow through the small probe passages and a flow rate of 1 liter/min was measured. To facilitate the cooling of the sample an aerodynamic tip containing a converging-diverging nozzle was fitted to the probe. For a measured sample flow rate of 1200 std. cc/min, a sample quench rate of 5000°C/millisecond was estimated while withdrawing sample from combustion zone at ~ 2000°K.

The thermocouple wires were of 0.1 mm dia. Pt vs Pt + 13% Rh. The junction was made by spot welding the wires approximately 2 mm away from the supporting ceramic stem to reduce conduction loss. To prevent surface catalysis, the exposed wires were coated with silica in a silicone oil flame. Correction for error in gas temperature measurement arising from loss of heat from the junction due to radiation was applied by using the relation in [30]. Maximum radiation loss encountered was in excess of 200°K.

To prevent the water vapor interference problem in the analysis by NDIR instruments, it was necessary to condense as much of the water vapor out of the sample as possible. The sample was passed through two cooling columns with continuous circulation of ice water, a dry ice bath, and a chemical Drierite. The comparatively large volume of the cooling system and small sample flow passages in the probe tend to increase the response time of the instruments. In order to minimize this response time and to supply enough sample flow rate to gas analyzers, it was necessary to employ an auxilliary diaphragm pump (Fig. 9). Due to

the suction from the sample handling diaphragm pumps, the cooling system was kept at about 12" Hg vacuum. To prevent the atmospheric air leaking into the system and diluting the sample, all glass joints were properly greased and all joints with teflon tubing were tightly wrapped with copper wire. The system was also leak checked to make sure that the leakage rate was negligible. Only teflon and stainless steel tubing were used for sample handling to prevent possible adsorption of certain species by other tubing materials.

It was assumed that negligible amount of condensable hydrocarbon products would be formed during the combustion of methane so that no separately heated line leading to hydrocarbon instrument was provided and a gas sample directly from the cooling system was supplied to the hydrocarbon instrument. No change in the hydrocarbon reading was observed when the sample line to the hydrocarbon instrument was connected directly, bypassing the cooling system.

2.3 Gas Analysis Instrumentation

The requirements of the gas analysis instrumentation for this work were significantly more demanding than those of the equipment commonly used for simple exhaust analyses of automotive engines. Not only must the instruments be capable of measuring accurately the extremely low concentrations of certain species, characteristic of the gas turbine exhaust, they are also called upon to manifest the same accuracy while analyzing the extremely high concentrations of the same species characteristic of the samples extracted from a zone of combustion. These requirements were satisfied well by a set of analyzers

from Beckman Instruments, Inc. The analyzer train consisted of

(i) Beckman model 315A NDIR CO analyzer with a long path sample cell of 40-1/2" for analysis of low concentrations and a short path sample cell of 1/8" for analysis of high concentrations. Of the five concentration ranges covered by the instrument, the lowest was 0-100 ppm CO in N_2 and the highest was 0-5% CO in N_2 .

(ii) Beckman model 106E total hydrocarbon analyzer employing a flame ionization detection technique, capable of measuring accurately from 10^4 ppm of equivalent hexane in N_2 down to 1 ppm in four ranges. Fortunately, due to the low hexane equivalence of methane (6 ppm CH_4 = 1 ppm C_6H_{14}[23]), no dilution of sample with N_2 was necessary while taking data near the fuel nozzle. This had to be done while taking data with liquid heptane as fuel in a previous investigation [18].

(iii) Beckman model 315 NDIR CO_2 analyzer with sample cell length of 1/8" covering a range 0-15% CO_2 in N_2 .

(iv) Beckman model 715 oxygen monitor employing an electrochemical transducer technique for analyzing the O_2 concentration in samples, with two ranges covering 0-5% and 0-25% O_2 by volume.

(v) At the outset of this experimental work, a Beckman model 315 NDIR NO analyzer with sample cell lengths of 13-1/2" and 7" was employed to measure NO . The lowest range was

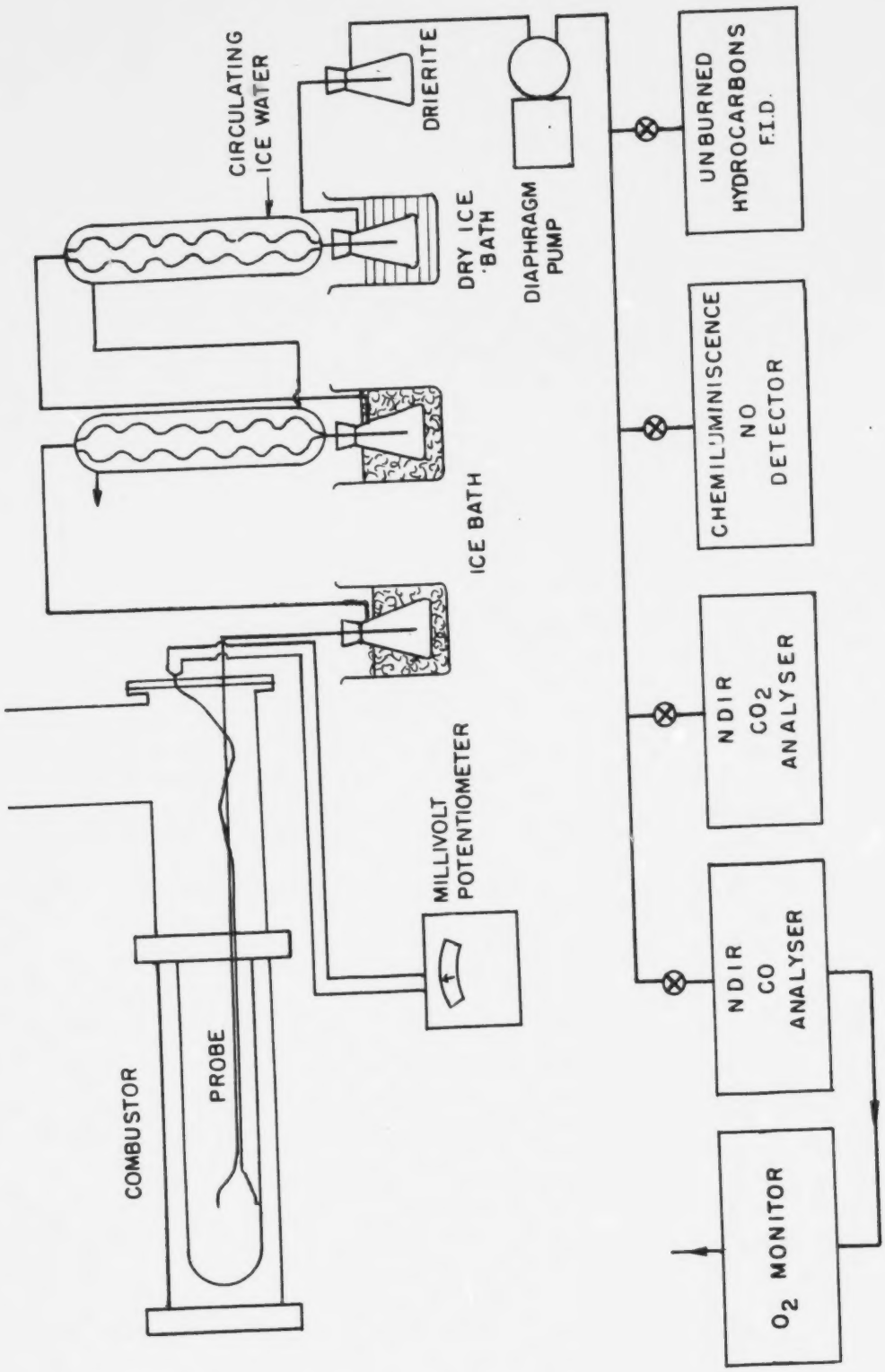

Figure 9. Sample Cooling System and Analyzer Train

0-500 ppm NO in N_2 . However, this instrument was soon found unsuitable for the extremely low concentrations of NO found throughout the combustor.

Fortunately, a recently developed NO detector exploiting the chemiluminescence of NO + ozone reaction [24] and capable of detecting NO concentrations down to a fraction of a part per million was on hand and was successfully used for this purpose. The fast response of the new detector and its immunity from water vapor interference problem were of much value for this investigation.

The calibration gases were supplied as trace gases in N_2 by the Scott Research Laboratories, the Matheson Co., and the Baker Chemical Co. N_2 was used as purge gas and for zeroing the instruments. The calibration gases, the sample cells, and the amplifier section were all housed in individual portable cabinets together with a sample handling system consisting of a diaphragm pump, rotameters, pressure gauges, and stainless steel valves and fittings.

Since the O_2 monitor was found to operate most satisfactorily when sample was supplied at near atmospheric pressure, it was connected to the exhaust from the CO NDIR analyzer. Figure 9 shows the layout of the sample handling system and the analyzer train.

2.4 The Test Procedure

Gas samples, taken at 60 locations in the combustor covering various axial and radial distances, for the 4 cases involving two nozzles and two equivalence ratios were analyzed for CO , CO_2 ,

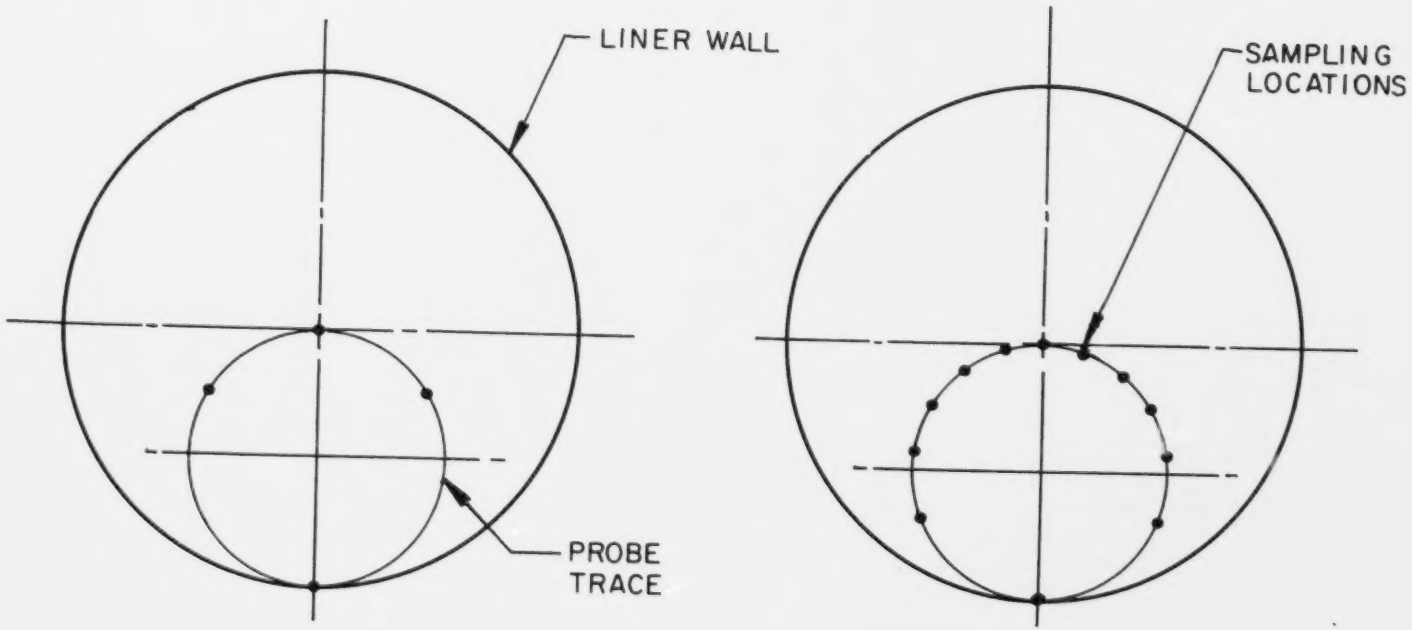

(i) RADIAL SAMPLING LOCATIONS AT 1/2", 1", 1 1/2", 2", 2 1/2", 4", 6" AND 8" AXIAL STATIONS

(ii) RADIAL SAMPLING LOCATIONS AT 3" AND 12" AXIAL STATIONS

Figure 10. Probe Trace and Sampling Locations Within the Combustor

O_2 , NO and unburned hydrocarbons. For each nozzle the overall equivalence ratios φ_o = 0.2 and 0.27 were investigated. The methane flow in all the four cases was kept constant at 4 lbm/hr and the variation in equivalence ratio was obtained by change in airflow rate.

In the selection of sampling locations, compromise had to be made between considerations of time involved for collection of data and minimum number of points required to obtain comprehensive results. The relatively large volume of the sample cooling system and sample lines compared to the minute flow passages of the probe resulted in sampling response time of approximately 2 min. Also, since the sample flow rate was so small, it was not possible to operate all the analyzers simultaneously. Due to these difficulties the total time taken for analysis of all the 5 species mentioned above for a given location of the probe was 6 to 8 minutes. Samples were taken for both clockwise and anticlockwise rotation of the probe. Figure 10 shows a map of sampling locations.

Although the data collected at these 60 locations yielded sufficient information for satisfactory interpretation of CO , CO_2 , O_2 and unburned hydrocarbon concentrations, it was found utterly inconclusive for NO concentrations. It was conjectured that the small number of sampling locations in each plane was not sufficiently representative of the average flux of NO concentration through that section. Also, the direct measurement of temperature presented considerable difficulty. The uncooled stainless steel tube carrying the thermocouple wires became distorted at flame temperatures and the delicate ceramic stem broke off several times due to interference

with the protruding ignitor electrode. Due to these experimental difficulties the more detailed measurements of NO concentrations and temperatures were performed separately for only one of the four cases of low velocity nozzle and $\varphi_o = 0.27$.

Difficulties were also encountered in stabilizing the flame with increasing airflow rates, especially for the case of high velocity nozzle. Actually $\varphi_o = 0.2$ was nearly the lowest equivalence ratio that could be attained in the case of high velocity nozzle before flame blowout. Stability was considerably improved with the low velocity nozzle. It was found that both the axial location and azimuthal orientation of the nozzles had significant influence on flame stability and lean blowout limit. Both were improved by locating the nozzle holes further away from the liner dome in the small distance (0 to 1/2" from the dome) through which such an axial movement was possible. It is believed that the air jets coming in through the radial slots in the dome tend to blow off the gaseous fuel jets if the nozzle holes are located too close to the dome. The better flame stability associated with low velocity nozzle was attributed to a more centralized fuel distribution resulting from relatively smaller penetration of fuel jets.

Since the air coming in through the slots in the dome is given virtually no swirl component of velocity in this design, the recirculation essential for flame stability is established by air coming through the first circumferential row of holes in the liner.

As would be expected, unstable combustion in the liner induced noticeable fluctuations of fuel flow in the case of low velocity nozzle

as observed in rotameter float position and pressure gauge. No such upstream influence was noticed for the case of high velocity nozzle since choked flow conditions at fuel nozzle were established.

During a continuous run and stable flame in the primary zone the reproduceability of concentration data was very good for all species - concentrations at a given location remained practically unchanged under such conditions. However, it deteriorated for data collected on separate runs. No estimates of reproduceability of data are made since most of the data was collected during continuous runs for each of the four cases.

A few of the samples were also analyzed for any presence of NO_2 arising from oxidation of NO in the combustor or the sample lines. An ultraviolet absorption technique was used for NO_2 detection [25] . The concentration of NO_2 , if any, was found to be below the level of detection (5 ppm) of the instrument for all cases.

After more than 50 hours of operation, no trace of carbon deposited in sample lines was found.

2.5 Test Results

The gas composition and temperature data obtained at various points in the combustor together with information deduced therefrom are presented graphically in Figs. 11 through 42. The averaged local concentration of a species at an axial station was obtained by averaging over the data taken at points in that plane. The radial distributions of concentrations, equivalence ratio and temperature are presented only for those axial stations where data at twelve points were obtained.

As mentioned earlier, the data for CO, CO_2, hydrocarbons and O_2 concentrations are presented for all the four cases investigated, namely, the combinations of two nozzles and two equivalence ratios. However, data for NO concentrations and temperature are presented for the only case of low velocity nozzle and $\varphi_o = 0.27$. Comparisons which lead to an understanding of the role of various factors such as overall equivalence ratio, gas injection velocity and fuel properties in determination of emission levels are also presented.

3. THE DISCUSSION OF RESULTS

Combustion in a gas turbine burner is a myriad of simultaneously occurring complex physical and chemical processes. The identification and detailed study of these individual processes have not lead to a complete understanding of gas turbine combustion. This state of affairs has resulted in widespread use of empiricism in this field [26]. In the latter practice a detailed study of the component processes as well as a qualitative understanding of their interaction in a practical combustion system have been of considerable importance. The discussion of results presented in this section is to a large extent qualitative in nature. It is arranged in three parts as follows:

3.1 The Influences of Overall Equivalence Ratio, Fuel Injection Velocity and Fuel Properties on the Axial Distributions of Averaged CO_2, CO and Unburned Hydrocarbons Concentrations.

3.2 The Axial Distributions of Averaged Local Equivalence Ratio and Air Flow.

3.3 The Problem of NO Formation.

3.1 The Axial Distributions of Averaged CO_2, CO and Hydrocarbons:

The trends observed in the axial distributions of centerline and average CO, CO_2 and unburned hydrocarbons concentrations are similar to those observed in a previous investigation with liquid fuel [18]. This serves to support the assertion made previously [18] that the production of pollutants in gas turbine combustors is governed by aerothermochemical processes.

An examination of averaged CO_2, CO and unburned hydrocarbon[1] concentration profiles for a single equivalence ratio in Fig. 11 reveals a qualitative resemblance to those that would obtain for a truly one-dimensional reacting flow for most of the combustor length. The departures from this behavior observed in regions very close to the fuel nozzle (< 1") may result from recirculating flow pattern and the method of taking simple average of data points in a plane. Outside this region, however, the initial stage of the precipitous decline in hydrocarbons concentration is accompanied by production of both CO and CO_2. The CO concentration soon reaches a peak and then declines, presumably because the rate of its consumption due to its conversion to CO_2 exceeds the rate of its formation due to the combustion of methane. The peak in CO_2 concentration is reached when the rate of its increase due to combustion of methane and CO equals the rate of its decrease due to dilution by addition of secondary air. In the latter part of the combustor, the decrease in CO concentration appears to be due both to chemical reaction and dilution since the rate of disappearance of CO is greater than what would be obtained for dilution alone.

The influences on the trends described above, of the overall equivalence ratio, the fuel injection velocity and the fuel properties will now be discussed individually.

---

[1]Unless otherwise mentioned, the hydrocarbon mole fractions are expressed as equivalent hexane mole fractions.

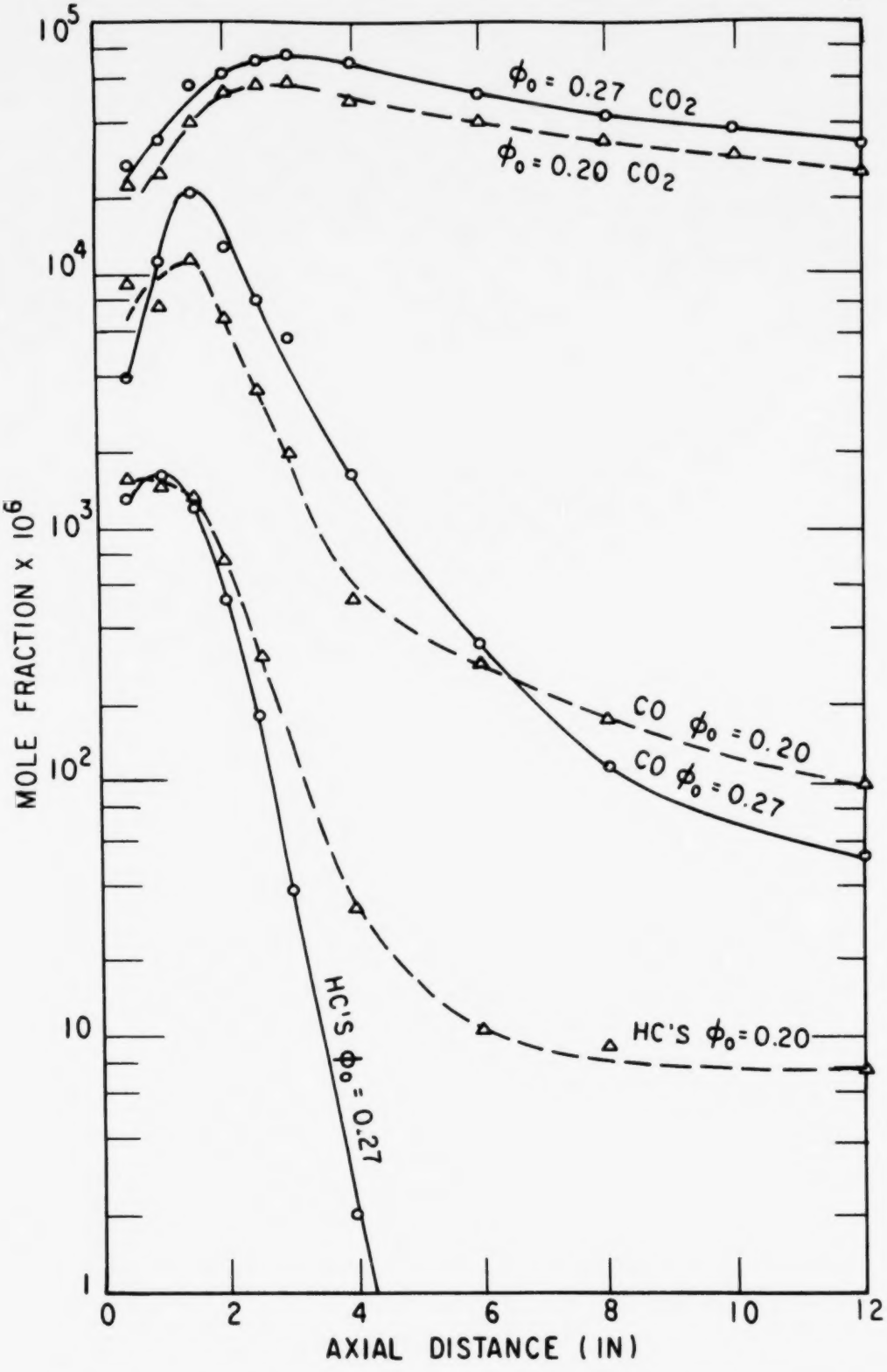

Figure 11. Axial Distribution of Averaged CO_2, CO and Hydrocarbons - Low Velocity Nozzle

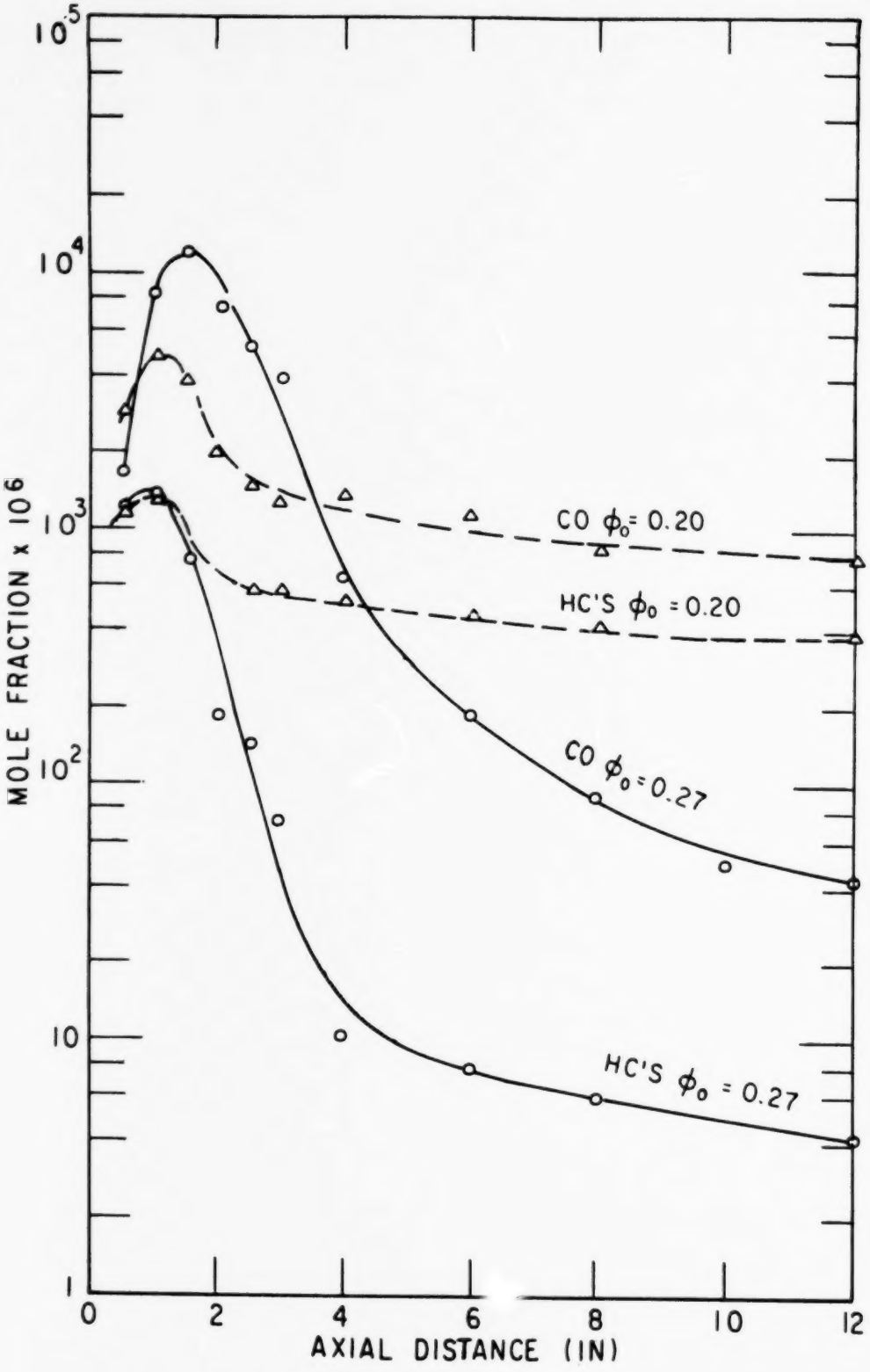

Figure 12. Axial Distribution of Averaged CO and Hydrocarbons - High Velocity Nozzle

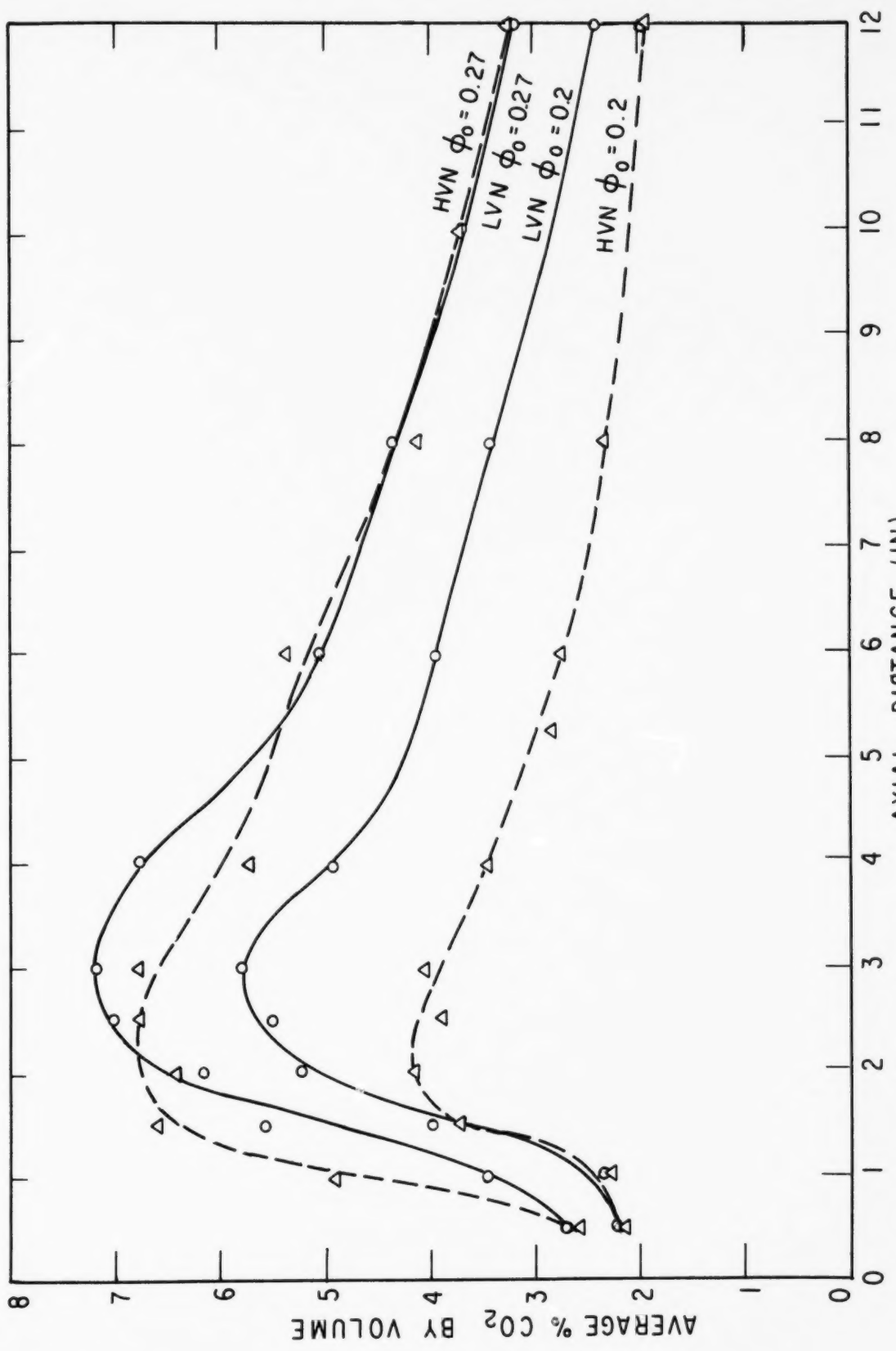

Figure 13. Axial Distribution of Averaged CO_2

3.1.1 The Effect of Overall Equivalence Ratio

The influence of the overall equivalence ratio, which is roughly the measure of load on a turbine engine, was fully investigated in previous experiments with liquid fuel [18]. The results obtained in this investigation are very similar to those obtained previously.

Figure 11 shows a comparison of trends for the two equivalence ratios for the case of low velocity nozzle; Fig. 12 shows these trends for the high velocity nozzle and Fig. 13 is a comparison of axial distributions of averaged CO_2 concentrations for the four cases.

Since the decrease in equivalence ratio was accomplished by increase in airflow, with no change in fuel flow, it would be expected that primary zone would operate leaner. This is evidenced by lower levels of CO_2 for each nozzle throughout the combustor (Fig. 13) and lower level of CO in the primary zone (less than about 3" from the fuel nozzle) (Fig. 11) as the overall equivalence ratio is decreased. It is to be noted that this observation is in qualitative agreement with consideration of chemical equilibrium.

In the secondary zone of the combustor, however, the addition of diluent air rapidly cools the products of combustion which tends to slow the oxidation of CO. This effect is seen in Fig. 11 for the case of low velocity nozzle. Thus, after a certain point the CO levels for low overall equivalence ratio operation exceed those for high equivalence ratio operation and this explains the appearance of higher CO emissions with decreasing load in operational turbine engines (Table III).

A similar effect is observed in the unburned hydrocarbons concentrations (Fig. 11). Although the higher reactivity of the latter

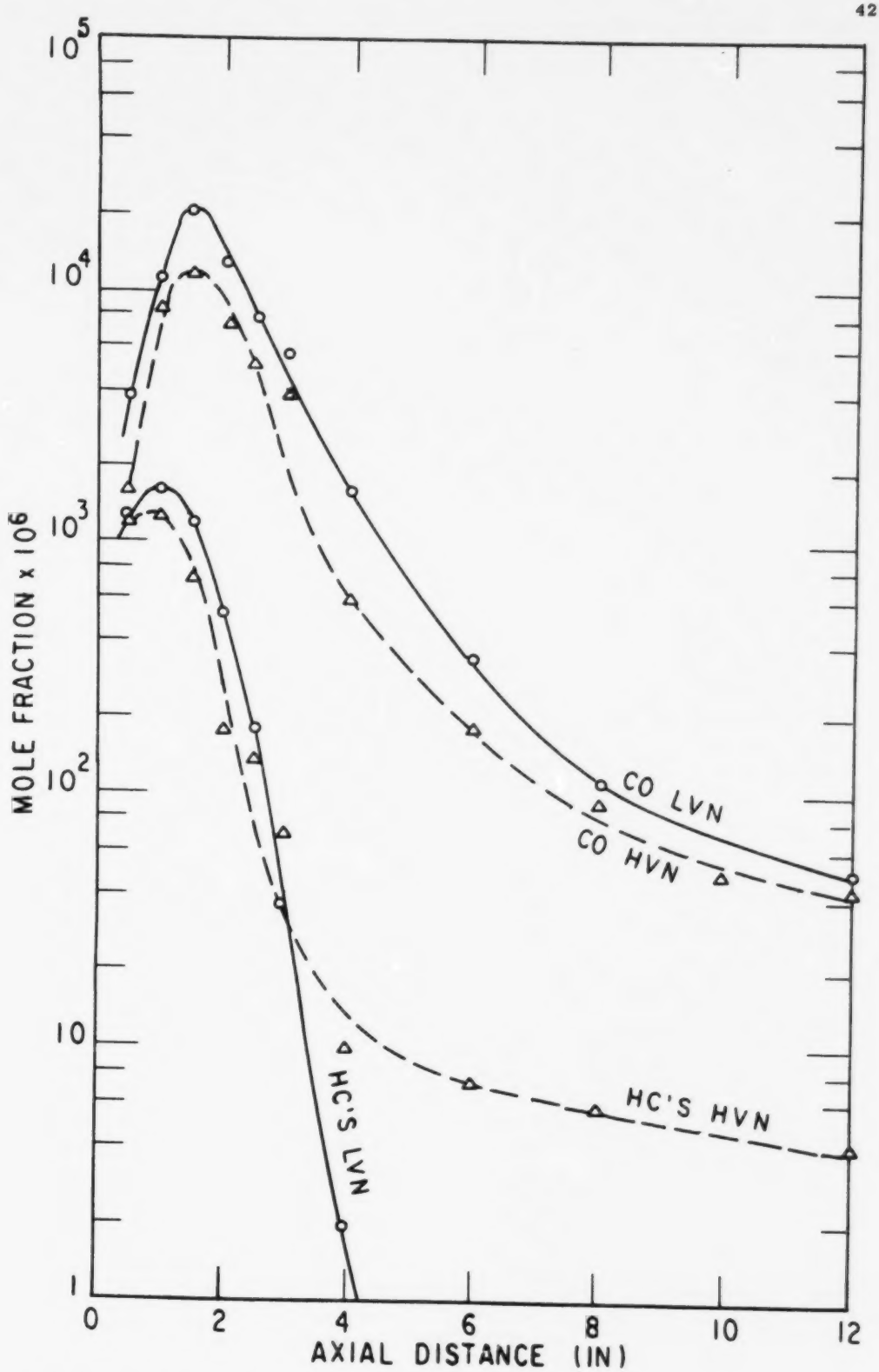

Figure 14. Axial Distribution of Averaged CO and Hydrocarbons $\varphi_o = 0.27$

compared to CO permits its more complete oxidation. The exit plane concentration of unburned hydrocarbons for $\varphi_o = 0.27$ in this case was found to be practically zero while that for $\varphi_o = 0.20$ was detected at less than 10 ppm.

The markedly different trends obtained for the case of $\varphi_o = 0.20$, high velocity nozzle (Fig. 12) require additional considerations for their explanation as discussed in the next section.

3.1.2 The Effect of Injection Velocity

Figure 14 shows the comparison of average CO and unburned hydrocarbons profiles obtained for the two nozzles at $\varphi_o = 0.27$. The peak concentrations of average CO, CO_2 (Fig. 13) and unburned hydrocarbons are lower for the high velocity nozzle. Since both the fuel and airflow rates are the same in these cases, it may be surmised that a greater penetration of fuel jets into the air stream permits better mixing of fuel and air and leads to leaner combustion.

An evidence of greater penetration of fuel jets for the case of high velocity nozzle is provided by a comparison of centerline gas composition with radial averages for the two nozzles (Fig. 15). For the case of low velocity nozzle, the centerline concentration of unburned hydrocarbons is comparable to radial averages near the fuel nozzle (< 1") and the CO concentration at the centerline is higher than the radial average in this region. However, for the case of high velocity nozzle, both CO and unburned hydrocarbon concentration are significantly lower at the centerline than the radial averages. Thus in the region in question (< 1" from the nozzle) the combustion takes place mostly near the liner wall for high velocity nozzle and mostly near the centerline for the low velocity nozzle. The low velocity

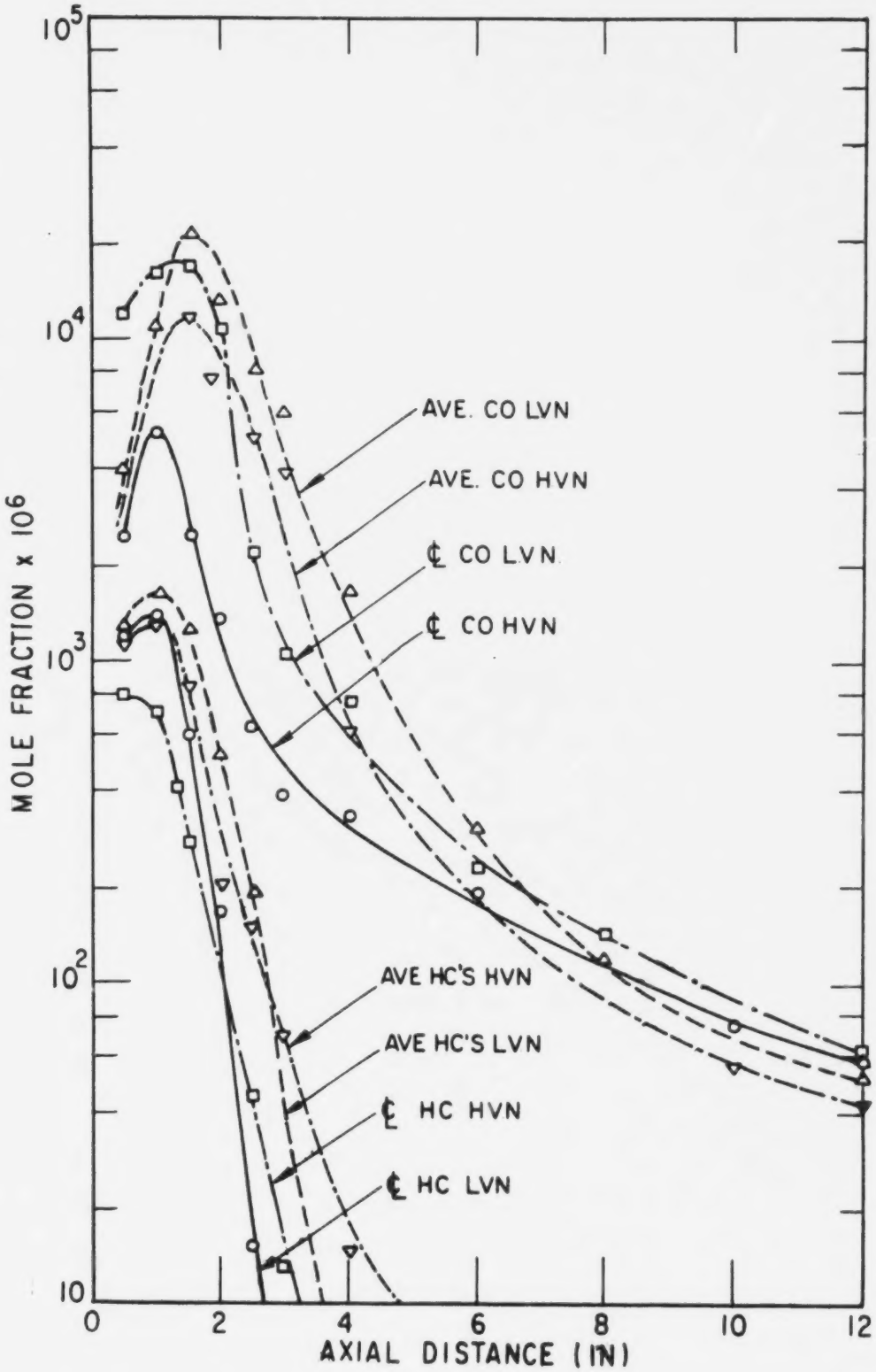

Figure 15. Axial Distribution of Averaged and Centerline CO and Hydrocarbons - $\varphi_o = 0.27$

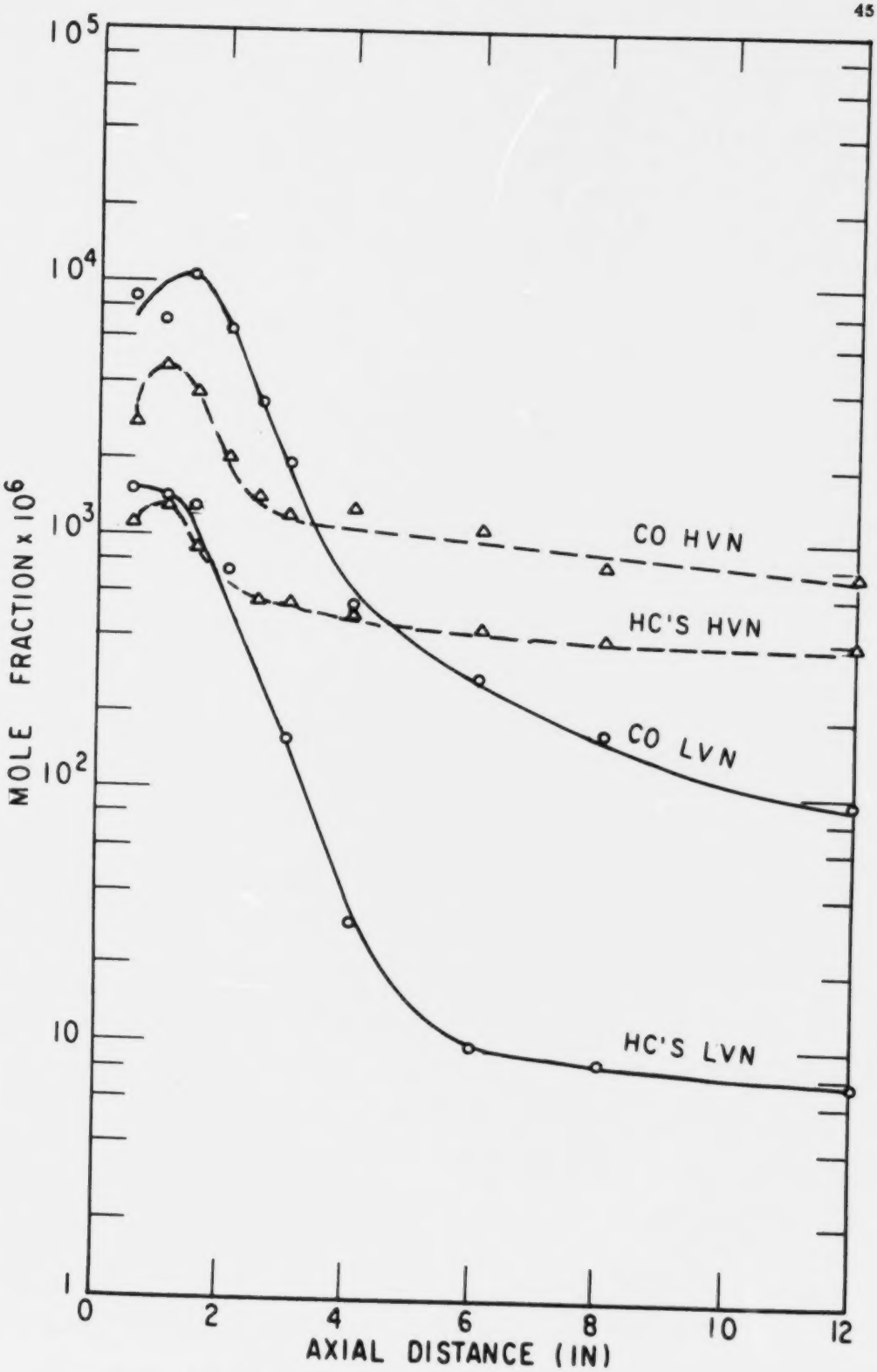

Figure 16. Axial Distribution of Averaged CO and Hydrocarbons $\varphi_o = 0.20$

nozzle gives a centralized fuel distribution.

It is a well known experience in gas turbine practice that anything that improves mixing of fuel with air in the primary zone tends to deteriorate the weak (lean) extinction performance of the combustor [26]. For this reason, as the airflow rate is increased, the weak extinction limit of high velocity nozzle is approached, characterized by regions in the primary zone where combustion reaction is prematurely quenched. This results in a sizeable proportion of fuel going through unburned and hence, a significantly low level of temperature throughout the combustor. It must be emphasized that the reason for the appearance of high exhaust concentration of CO and unburned hydrocarbons in this case is distinct from that discussed in the previous section. Here the reaction is locally quenched at regions in the primary zone itself while in the case of low velocity nozzle and $\varphi_o = 0.20$ quenching occurred in the latter part of the secondary zone (Fig. 16).

It appears that the heat release rate in the primary zone has marked influence on the distribution of airflow along the combustor. For the same total airflow through the combustor a lower heat release rate causes a higher percentage of the total airflow to enter into the primary zone. This observation is supported by experimental evidence and is discussed in a later section.

Finally, an examination of average CO_2 concentration profiles (Fig. 13) reveals that the peaks in CO_2 for high velocity nozzle occur earlier than those for the low velocity nozzle. This indicates that combustion reactions are completed in a shorter distance when high velocity nozzle is used.

3.1.3 The Effect of Fuel Properties

One of the primary objectives of this work was to investigate the essential differences between the air pollution characteristics of gaseous and liquid fuels used in the model combustor. For this purpose a comparison is made between the average CO and hydrocarbons profiles for $\varphi_o = 0.27$, low velocity nozzle and methane as fuel and those obtained previously [18] during experiments with heptane and $\varphi_o = 0.28$ (Fig. 17). The air and fuel flow rates for the two cases are comparable as shown below:

Fuel	$\dot{m}_f$ $\frac{lbm}{hr}$	$\dot{m}_a$ $\frac{lbm}{hr}$	$(A/F)_s$	φ_o
Heptane [18]	4.5	242	15.1	0.28
Methane	4.1	260	17.15	0.27

The qualitative features of burning gaseous fuel jets and liquid fuel droplets are fairly well understood. For the former, the mixing time is considerably smaller than the reaction time. For the latter, the mixing time may be comparable to or greater than the reaction time depending upon the droplet size, the volatility of the fuel and diffusivity of fuel vapor, among other parameters. Two important consequences of these distinctions are:

(i) The liquid fuel, after its injection into the chamber, requires greater residence time for complete combustion.

(ii) The local average equivalence ratio at which fuel droplets burn is higher than that encountered during the combustion of gaseous fuel jet with the same overall equivalence ratio.

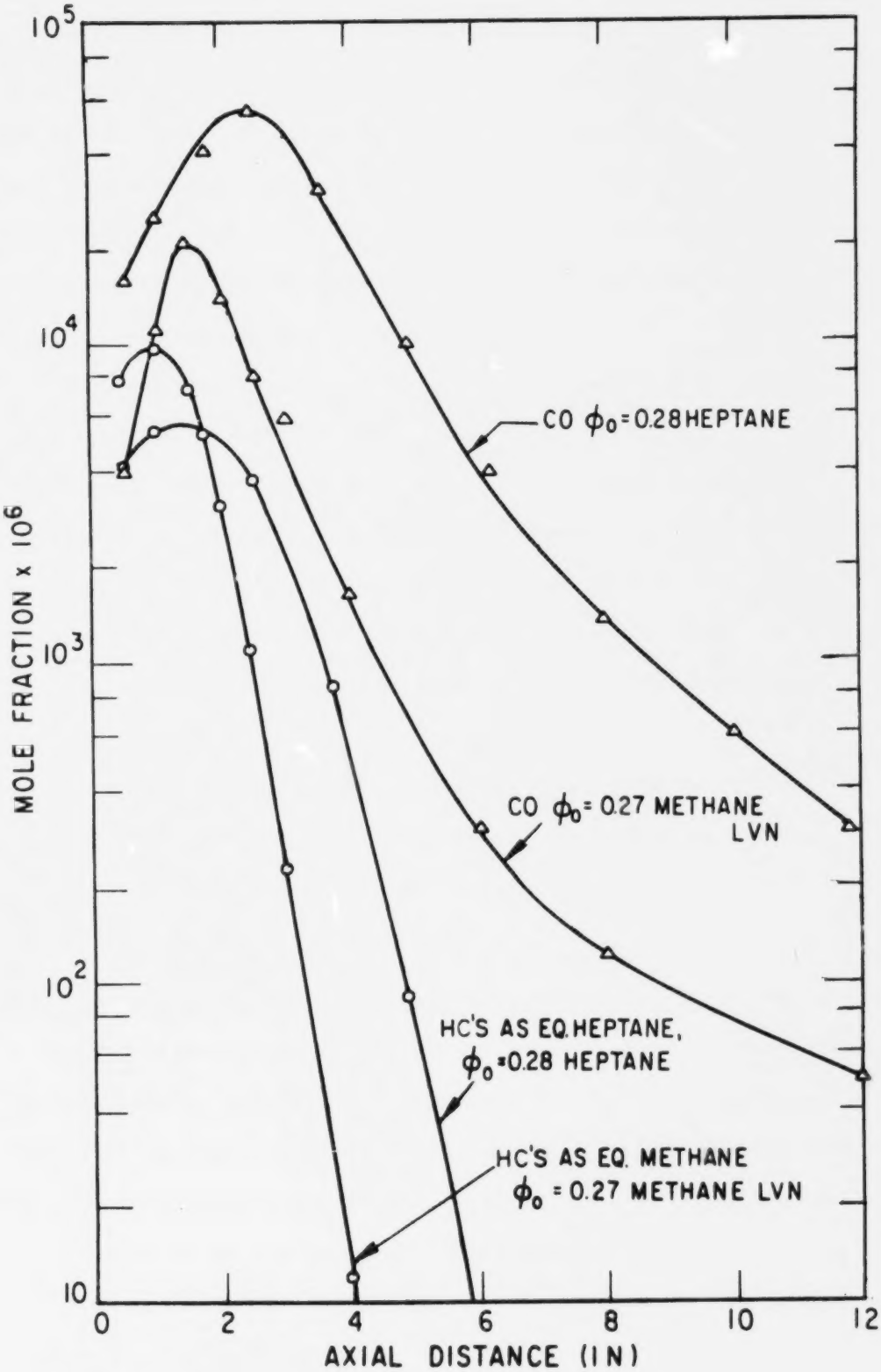

Figure 17. Comparison of Axial Distribution of Averaged CO and Hydrocarbons for Heptane and Methane

These two factors have important influence on air pollution characteristics of gas turbine combustors as seen from Fig. 17. In the primary zone, the higher level of CO concentration for heptane is a consequence of higher local average equivalence ratio of combustion. Although the rates of oxidation of CO in the secondary zone appear comparable for the two cases, the higher CO level continues beyond the exit plane for the liquid fuel.

The increased residence time required by liquid fuel for complete combustion is also evident from a comparison of hydrocarbons profiles for the two fuels (Fig. 17). For this purpose the hydrocarbons are expressed as mole fraction of fuels themselves rather than equivalent hexane mole fractions. It can be seen that the combustion of methane is completed in a much shorter distance. This also results in a downstream shift of peak CO concentration point for Heptane.

Both the lean combustion and shorter flame length encountered with the use of methane reduce the NO levels to significantly low values. This is discussed at greater length in the section on NO formation.

3.2 Axial Distribution of Averaged Local Equivalence Ratio and Airflow

An important parameter which provides an insight into the air and fuel distribution throughout the combustor is the local equivalence ratio. At any location in the combustor, if the concentrations of CO_2, CO and unburned hydrocarbons are known, the local equivalence ratio can be calculated from the formula derived in Appendix B. It is also possible to calculate what the mole fraction of O_2 should be at that location from Stoichiometric relations. A comparison of the

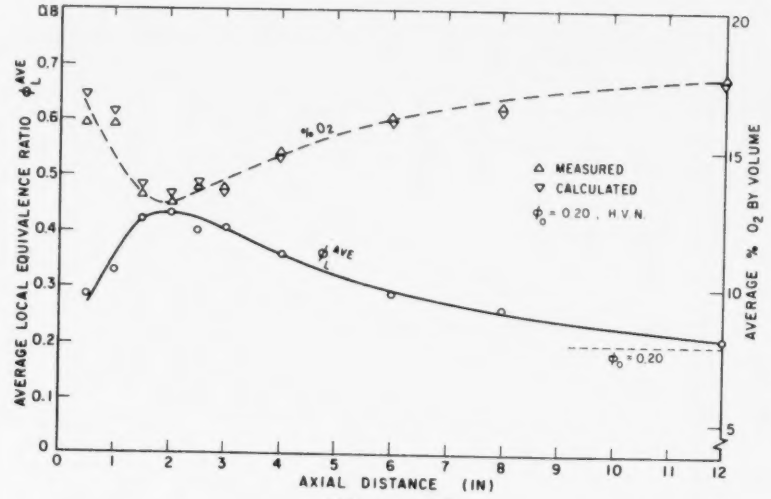

Figure 18

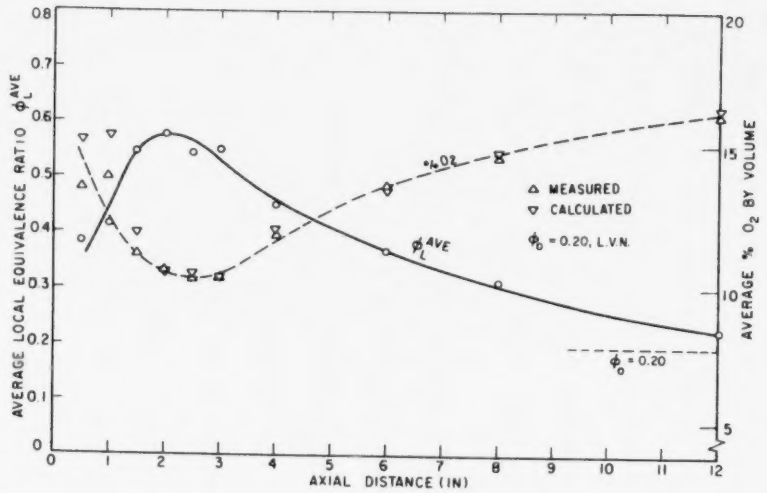

Figure 19

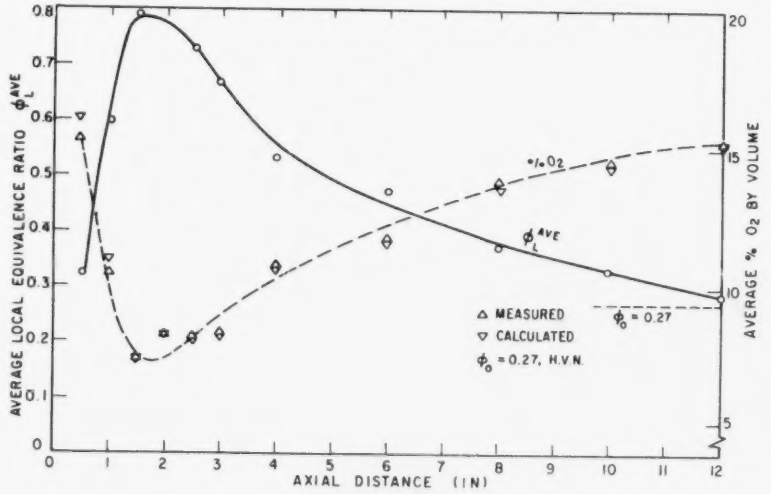

Figure 20

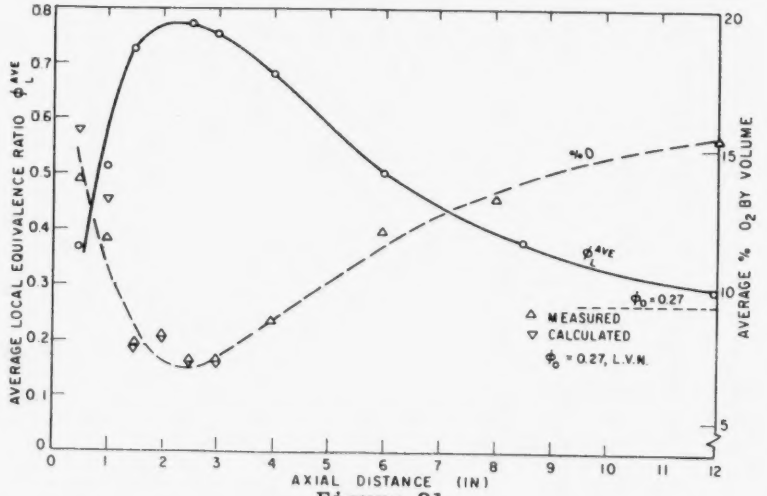

Figure 21

Axial Distribution of Averaged Local Equivalence Ratio and O_2

measured mole fraction of O_2 with that calculated then provides a check on all measured mole fractions and hence on the calculated value of the local equivalence ratio. At those locations where good agreement was obtained between measured and calculated mole fractions of O_2, the calculated local equivalence ratio was taken as accurate.

3.2.1 Axial Distribution of Averaged Local Equivalence Ratio

The axial profiles of averaged O_2 mole fractions and local equivalence ratios are plotted for the four cases involving two nozzles and two equivalence ratios in Figs. 18 through 21. It is noted that the agreement between measured and calculated values of O_2 is excellent for all axial stations beyond 2". However, there are marked discrepancies in regions closer to the fuel nozzle and the apparent dropping off of equivalence ratio in this region is fallacious. This apparently contradictory behavior of averaged local equivalence ratio and observed discrepancies between measured and calculated values of O_2 near the fuel nozzle are attributable to inhomogeneities present in the region in question. In Fig. 22, the axial distributions of averaged local equivalence ratios for the four cases are plotted. The weighted averages over a section of all data points in a plane were taken in preparation of Fig. 22.

In Figs. 23 and 24 the comparison between radial distribution of local equivalence ratio at 3" section is illustrated for both clockwise and counterclockwise rotation of the probe. The asymmetry in the radial distribution of local equivalence ratio for the two directions is noticeable. Since the fuel nozzle was provided with a filter and was also occasionally inspected to see if the holes were

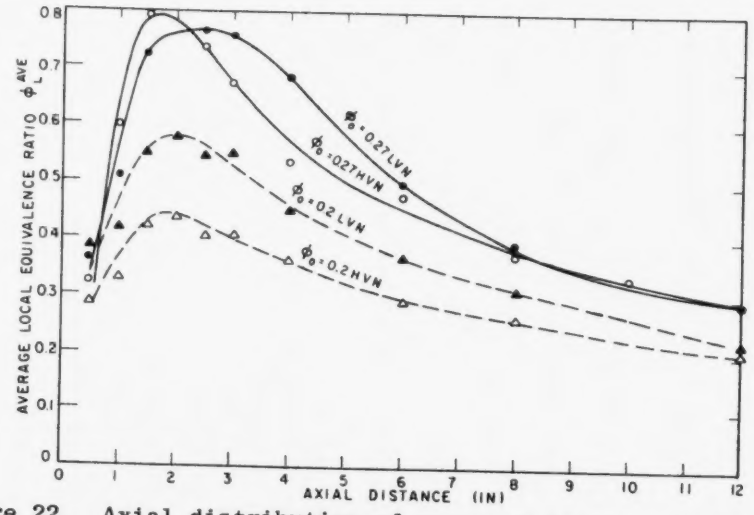

Figure 22. Axial distribution of averaged local equivalence ratio

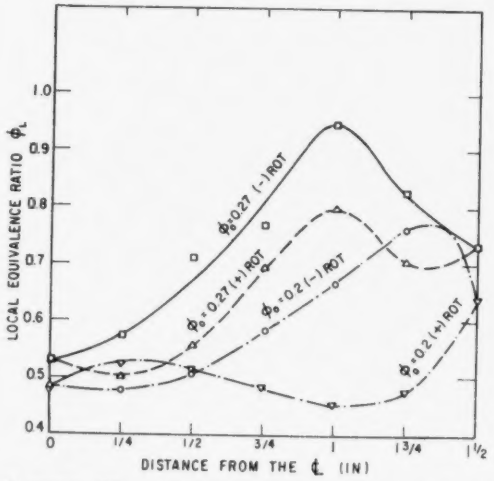

Figure 23. Radial equivalence ratio distribution at 3" axial station - L.V.N.

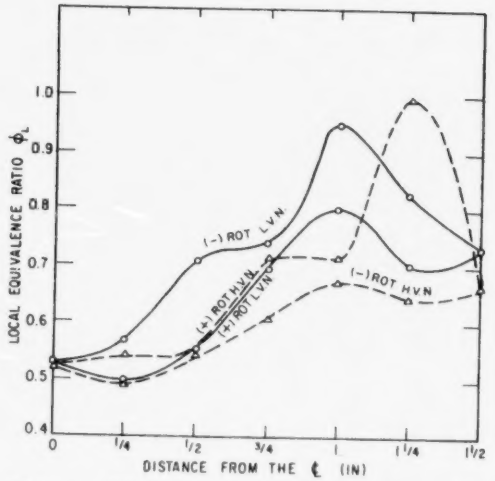

Figure 24. Radial equivalence ratio distribution at 3" axial station - φ_o = 0.27

blocked (which they never were), the fuel distribution must have been symmetric. Hence the observed effect must have been due to asymmetric airflow distribution which may arise either from eccentricity of the inconel liner with respect to the pyrex tube or from an asymmetric airflow distribution in the combustor head. It is seen from Fig. 24 that at 3" section, the equivalence ratio at most points is lower for the high velocity nozzle except close to the wall. The effect of increasing airflow rate is seen as lowering of local equivalence ratios at various points in Fig. 23.

3.2.2 Axial Airflow Distribution

An important parameter which can be derived from the axial distribution of averaged local equivalence ratio is the mass of air passing through a given axial station, expressed as a fraction of the total airflow. Denoting this fraction by x_a,

$$x_a = \frac{\dot{m}_a}{\dot{m}_{a,o}} = \frac{\dot{m}_a / \dot{m}_{a,o}}{\dot{m}_a / \dot{m}_a} = \frac{\varphi_o}{\varphi_L^{ave}}$$

where,

φ_o is the overall equivalence ratio

φ_L^{ave} is the average local equivalence ratio at that station

$\dot{m}_a$ = mass flow rate of air past that section

$\dot{m}_{a_o}$ = total mass flow rate of air

$\dot{m}_f$ = mass flow rate of fuel.

The axial distribution of x_a are shown in Fig. 25 for the four cases. In preparation of these curves the weighted averages over a section of the local equivalence ratio were used. Since the determination of local equivalence ratio is not accurate in the regions

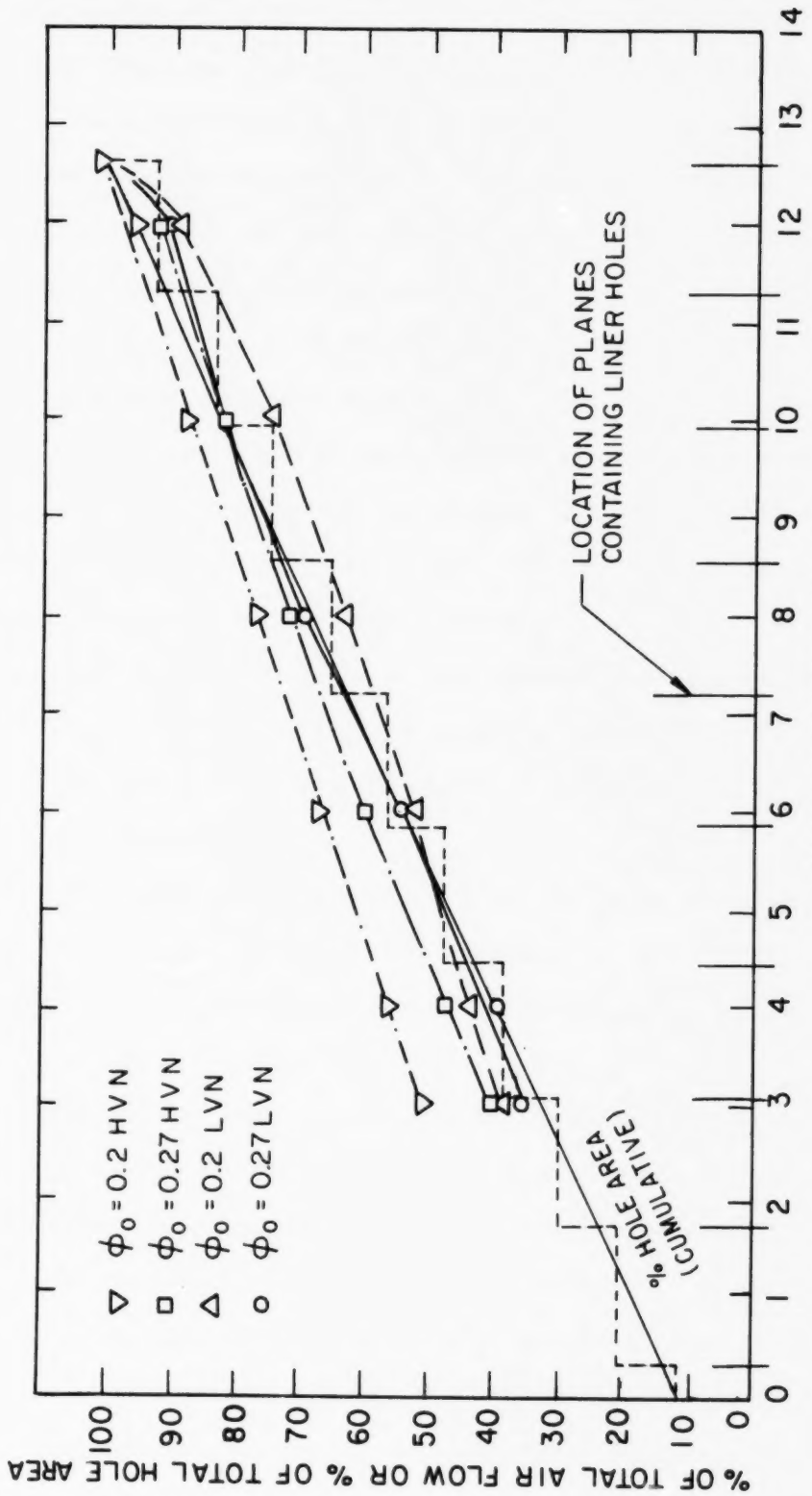
% OF TOTAL AIR FLOW OR % OF TOTAL HOLE AREA
AXIAL DISTANCE (IN)
LOCATION OF PLANES CONTAINING LINER HOLES
% HOLE AREA (CUMULATIVE)
ϕ_o = 0.2 HVN
ϕ_o = 0.27 HVN
ϕ_o = 0.2 LVN
ϕ_o = 0.27 LVN

Figure 25. Axial Air Flow Distribution

close to the nozzle due to inhomogeneities and also, the assumption of one-dimensional flow is questionable in this region, the curves of x_a are plotted only up to the 3" section. The accuracy of the airflow distribution predicted by these curves is consistent with the legitimacy of the averaging procedure used for determination of φ_L^{ave} and the one dimensional flow assumption.

In Fig. 25 the axial distributions of airflow for the four cases are compared with cumulative hole area. The slot area in the liner dome accounts for 11.5% of the total hole area. The contribution of the liner hole areas is represented both as a stepwise increase as well as an idealized linear increase. Several conclusions could be drawn by an examination of these curves:

(i) There must be an excessive flow through the slots in the liner dome in all four cases. This may be caused by two effects:
   (a) The dynamic pressure effect of incoming air from the combustor head
   (b) Larger orifice coefficient for a slot as compared to a circular hole due to the presence of one-dimensional vena contracta for a slot and two-dimensional vena contracta for a circular hole.

(ii) For the same heat release rate in the combustor, the effect of increasing the total airflow is to reduce the fraction of airflow through the holes in the early part of the secondary zone and increase that fraction for the latter part of the same (L.V.N.).

(iii) For the same airflow ($\varphi_o = 0.20$) the effect of decreasing the heat release rate (as in H.V.N.) is to increase the fraction of air entering the primary zone and reduce that entering from

the holes in the latter part of the secondary zone.

(iv) If the flow through the liner dome were to be shut off, a greater proportion of air would enter from the holes in the latter part of the combustor.

These conclusions are in qualitative agreement with those arrived at by Graves and Grobman [27] in their theoretical analysis of an idealized model of a tubular combustor.

The knowledge about the axial distribution of airflow in the combustor is very useful in the determination of the time histories of fluid elements under one-dimensional flow assumption. This is discussed in a later section.

3.3 The Problem of NO Formation

As mentioned previously, the data obtained for NO by analyses of gas samples withdrawn at 60 locations within the combustor were found to be inconclusive. The data presented here on NO concentrations and temperature were taken during a separate run for the only case of low velocity nozzle and $\varphi_o = 0.27$. Samples were withdrawn at 144 locations involving greater number of radial locations than before.

The radial distributions of NO concentrations and temperature at various axial stations are shown in Figs. 26 through 34 for both clockwise and counterclockwise rotation of probe. The data for NO concentrations corresponding to counterclockwise (-) rotation of the probe at several axial stations are replotted in Fig. 35. The significant radial gradients in NO concentrations observed in the primary zone together with vanishing of these gradients in the latter part of the secondary zone due to mixing with dilution air explain

the holes in the latter part of the secondary zone.

(iv) If the flow through the liner dome were to be shut off, a greater proportion of air would enter from the holes in the latter part of the combustor.

These conclusions are in qualitative agreement with those arrived at by Graves and Grobman [27] in their theoretical analysis of an idealized model of a tubular combustor.

The knowledge about the axial distribution of airflow in the combustor is very useful in the determination of the time histories of fluid elements under one-dimensional flow assumption. This is discussed in a later section.

3.3 The Problem of NO Formation

As mentioned previously, the data obtained for NO by analyses of gas samples withdrawn at 60 locations within the combustor were found to be inconclusive. The data presented here on NO concentrations and temperature were taken during a separate run for the only case of low velocity nozzle and $\varphi_o = 0.27$. Samples were withdrawn at 144 locations involving greater number of radial locations than before.

The radial distributions of NO concentrations and temperature at various axial stations are shown in Figs. 26 through 34 for both clockwise and counterclockwise rotation of probe. The data for NO concentrations corresponding to counterclockwise (-) rotation of the probe at several axial stations are replotted in Fig. 35. The significant radial gradients in NO concentrations observed in the primary zone together with vanishing of these gradients in the latter part of the secondary zone due to mixing with dilution air explain

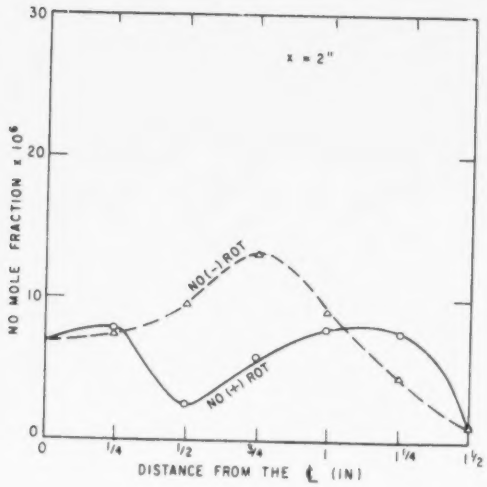

Figure 26

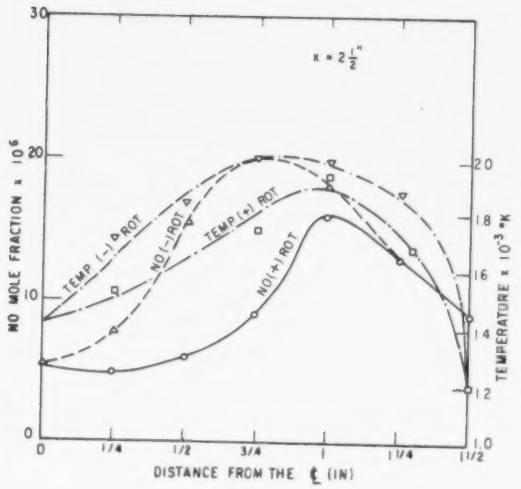

Figure 27

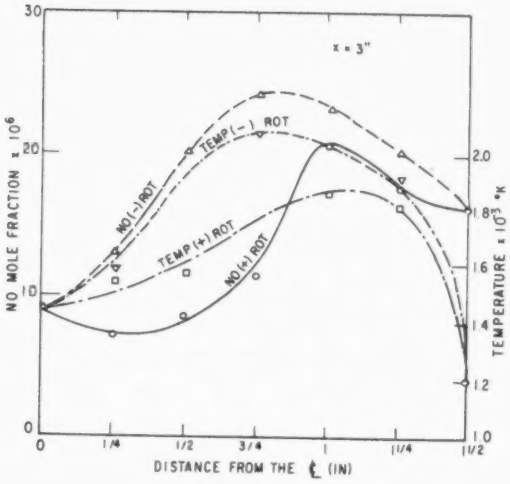

Figure 28

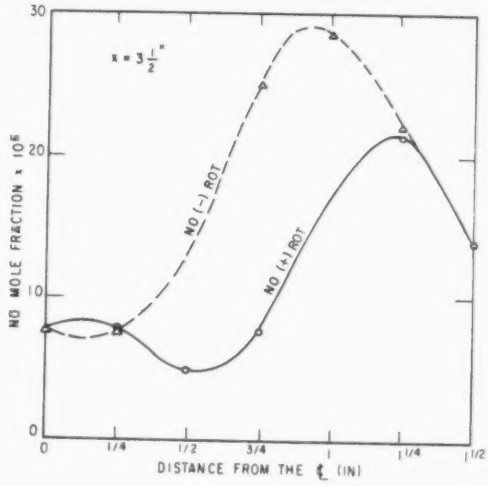

Figure 29

Radial Distribution of NO Concentration at Various Axial Stations - φ_o = 0.27, L.V.N.

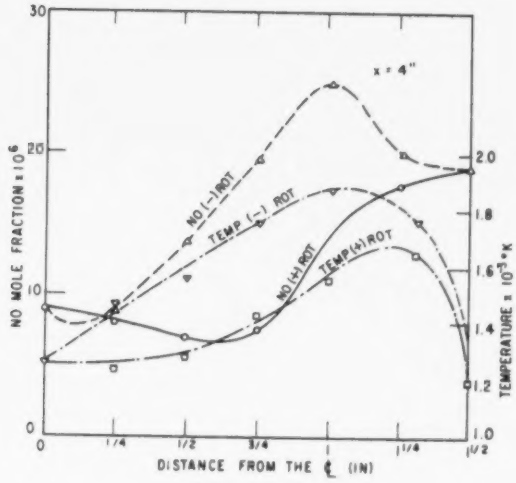

Figure 30

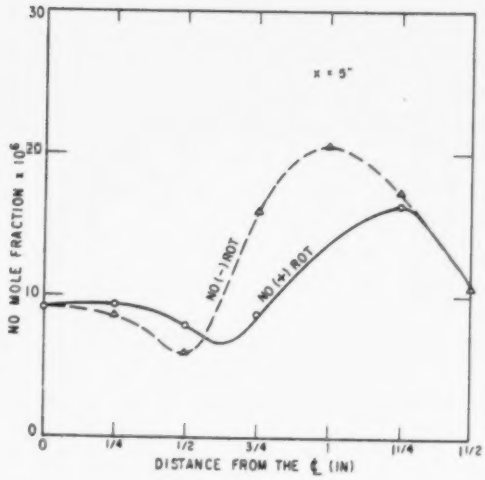

Figure 31

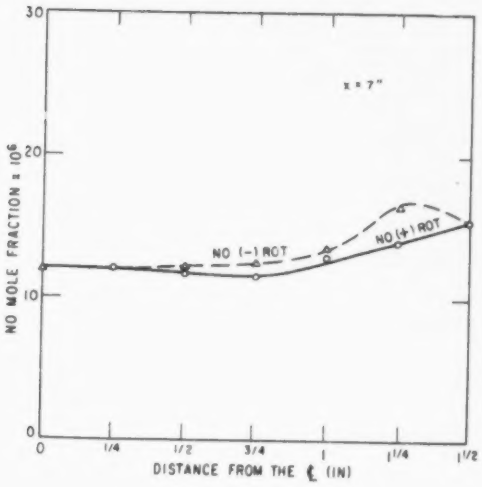

Figure 32

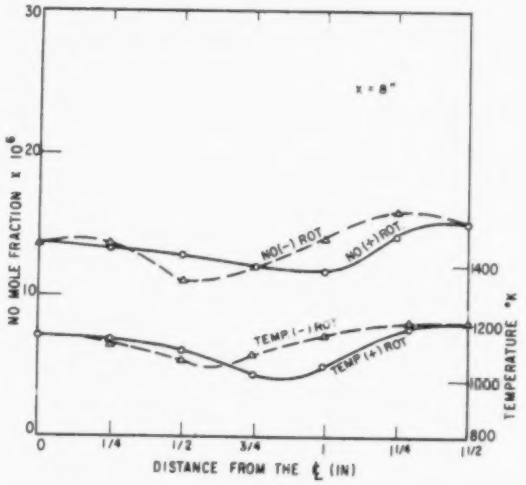

Figure 33

Radial Distribution of NO Concentration at Various Axial Stations - φ_o = 0.27, L.V.N.

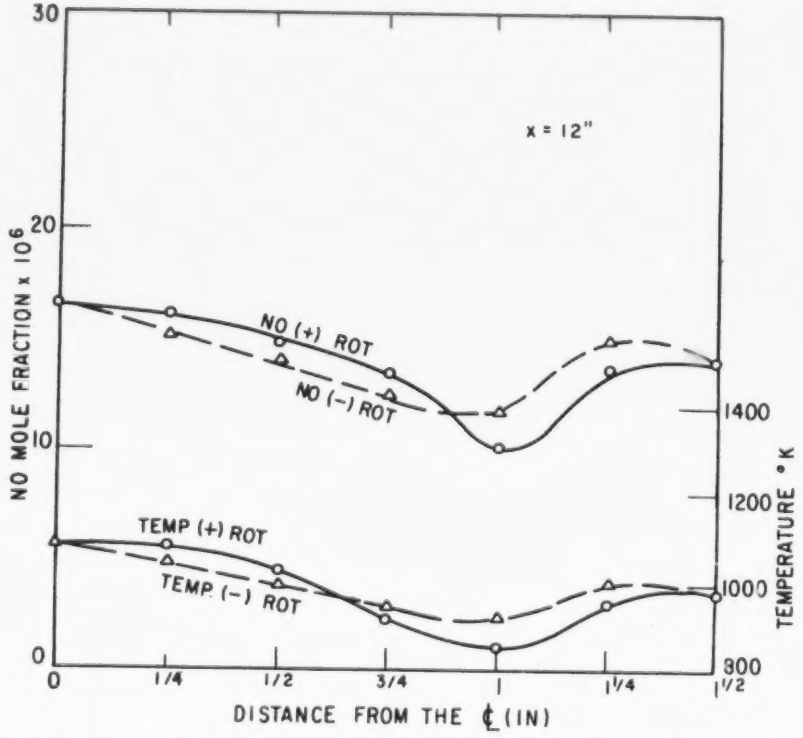

Figure 34. Radial distribution of NO concentration and temperature at 12" axial station - φ_o = 0.27, L.V.N.

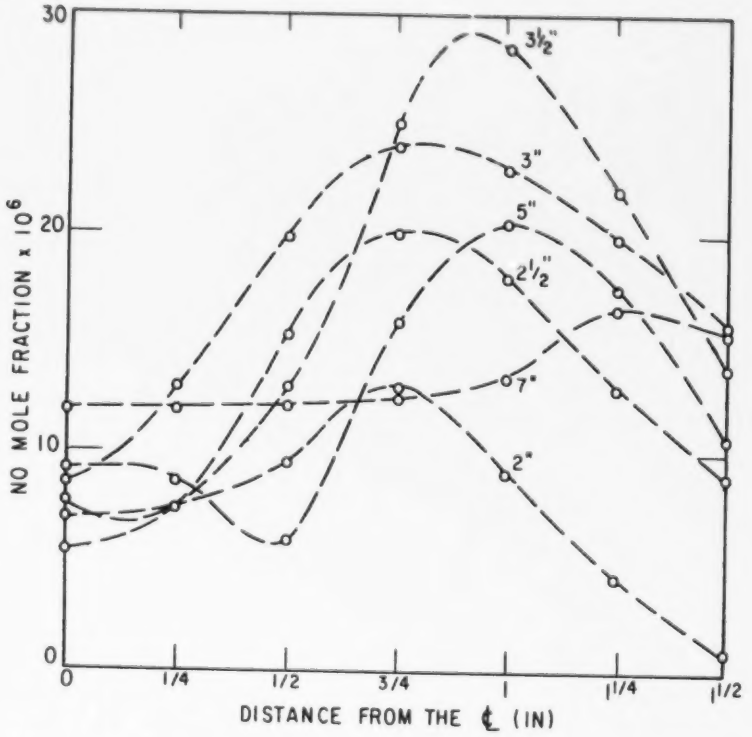

Figure 35. Radial distribution of NO concentration at various axial stations - φ_o = 0.27, L.V.N., negative rotation of probe

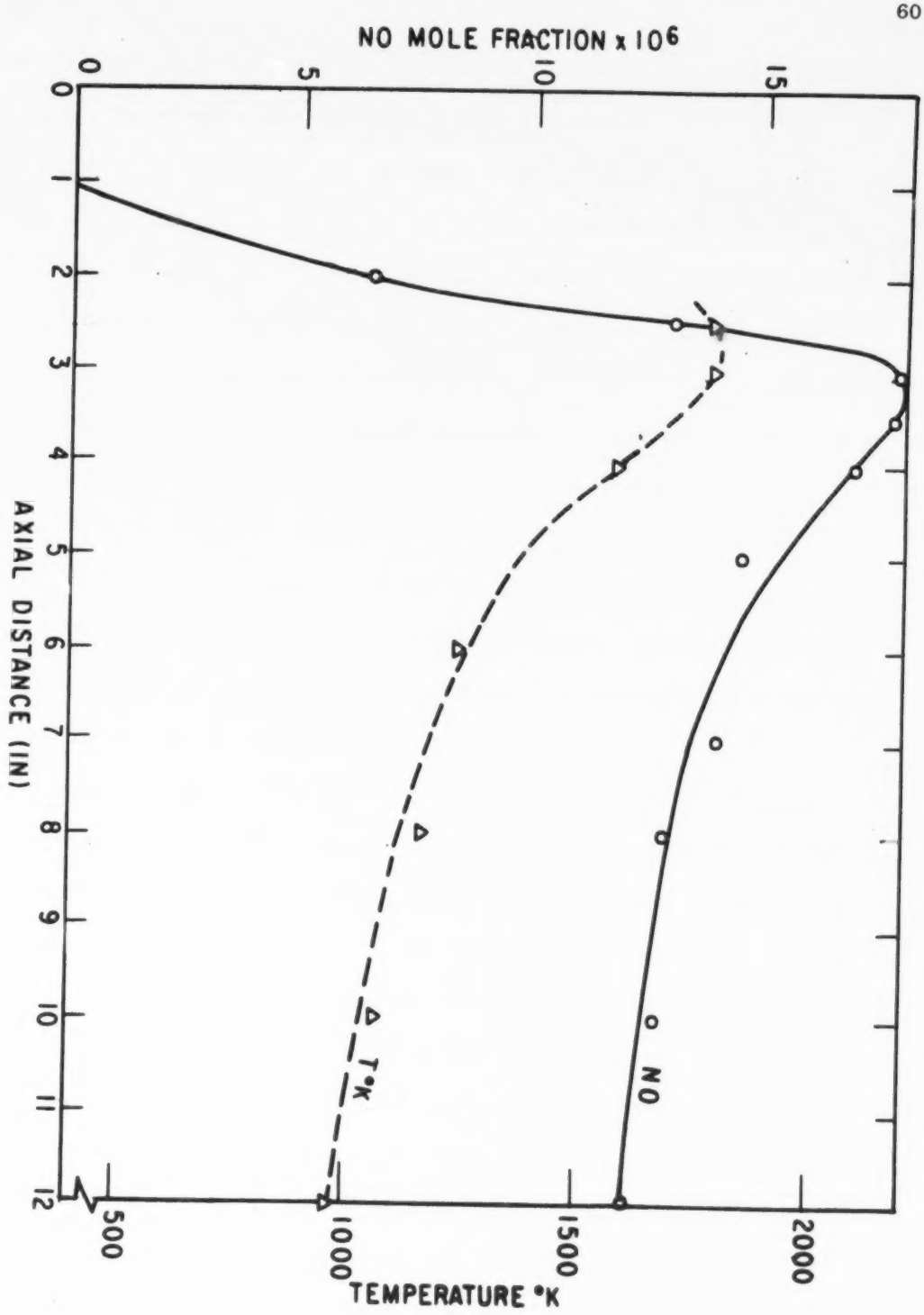

Figure 36. Axial Distribution of Averaged NO Concentration and Temperature - φ_o = 0.27, L.V.N.

the inconclusive nature of the data taken previously at only a few points. The weighted averages over a section of NO concentrations and temperature were calculated and these results are plotted in Fig. 36.

Unlike CO which continues to disappear due to chemical reactions throughout the secondary zone, the reactions involving NO are effectively frozen at the very outset of secondary zone and the observed slow decrease in averaged NO concentration is due rather to dilution by secondary air than to chemical reactions. Thus, while the exhaust emissions of CO and unburned hydrocarbons are determined by the extent to which the reactions bringing about their depletion are allowed to proceed, those of NO are governed by the extent to which its formation reactions are allowed to progress. Hence it is important to study the factors which influence the formation of NO in the primary zone of the combustor.

Figure 37 shows the concentrations of NO in the equilibrium products of methane-air combustion at adiabatic flame temperatures for several equivalence ratios. These data were obtained by the use of NASA CECS70 computer program for equilibrium thermodynamic properties. A comparison of equilibrium NO concentrations with those measured in the combustor indicates that the equilibrium NO concentrations are at least an order of magnitude greater than the measured values. It appears, therefore, that the levels of NO concentration are governed by the rate of its formation and the time interval over which this formation continues.

In order to obtain a rough estimate of the time scale involved in the combustor flow processes, a simplified one-dimensional model of the secondary zone was considered. Using the information about the

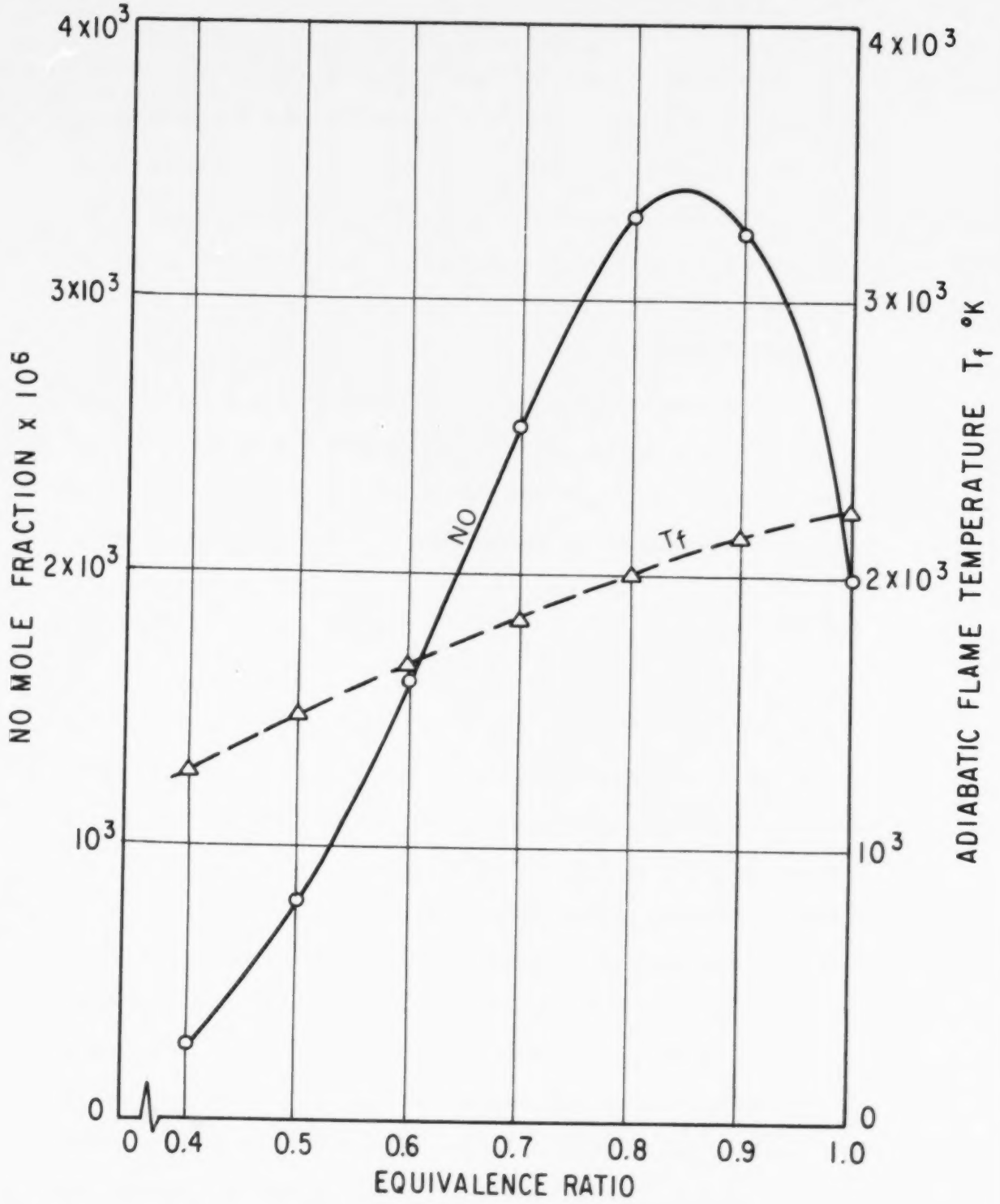

Figure 37. Equilibrium NO Concentration and Flame Temperature in Adiabatic Methane-Air Combustion - $T_{initial} = 298^{\circ}K$, p = 1 ata.

axial airflow distribution (Fig. 25) together with the total airflow rate through the combustor, the mass flow rates of the exhaust products across various sections in the secondary zone of the liner were computed. By considering the perfect gas relationship and assuming the pressure to be constant at 1•2 ata throughout the secondary zone, the axial averaged density distribution was derived from the measured averaged temperature profile (Fig. 36). By using this averaged density distribution and mass flow rate at various sections together with constant liner area, it was possible to calculate the axial distribution of average gas velocity at a section. The axial distributions of average density and velocity are shown in Fig. 38. With this knowledge of the axial velocity as a function of distance given as

$$V_{ave} = \frac{dx}{dt} = f(x)$$

and with an initial condition $t = 0$ at $x = 2\frac{1}{2}"$, the distance x was computed as a function of time by integration as shown in Fig. 38. Finally, using this distance-time curve it was possible to translate the axial distributions of various quantities such as average equivalence ratio, average concentrations and average temperature into the time histories of these quantities for a one-dimensional fluid element. These results are plotted in Fig. 39. It is seen that a typical time scale involved in the flow process is of the order of a few milliseconds. One might thus expect that the time interval during which a fluid element is subjected to high temperature in the primary zone would be approximately 3 to 5 milliseconds.

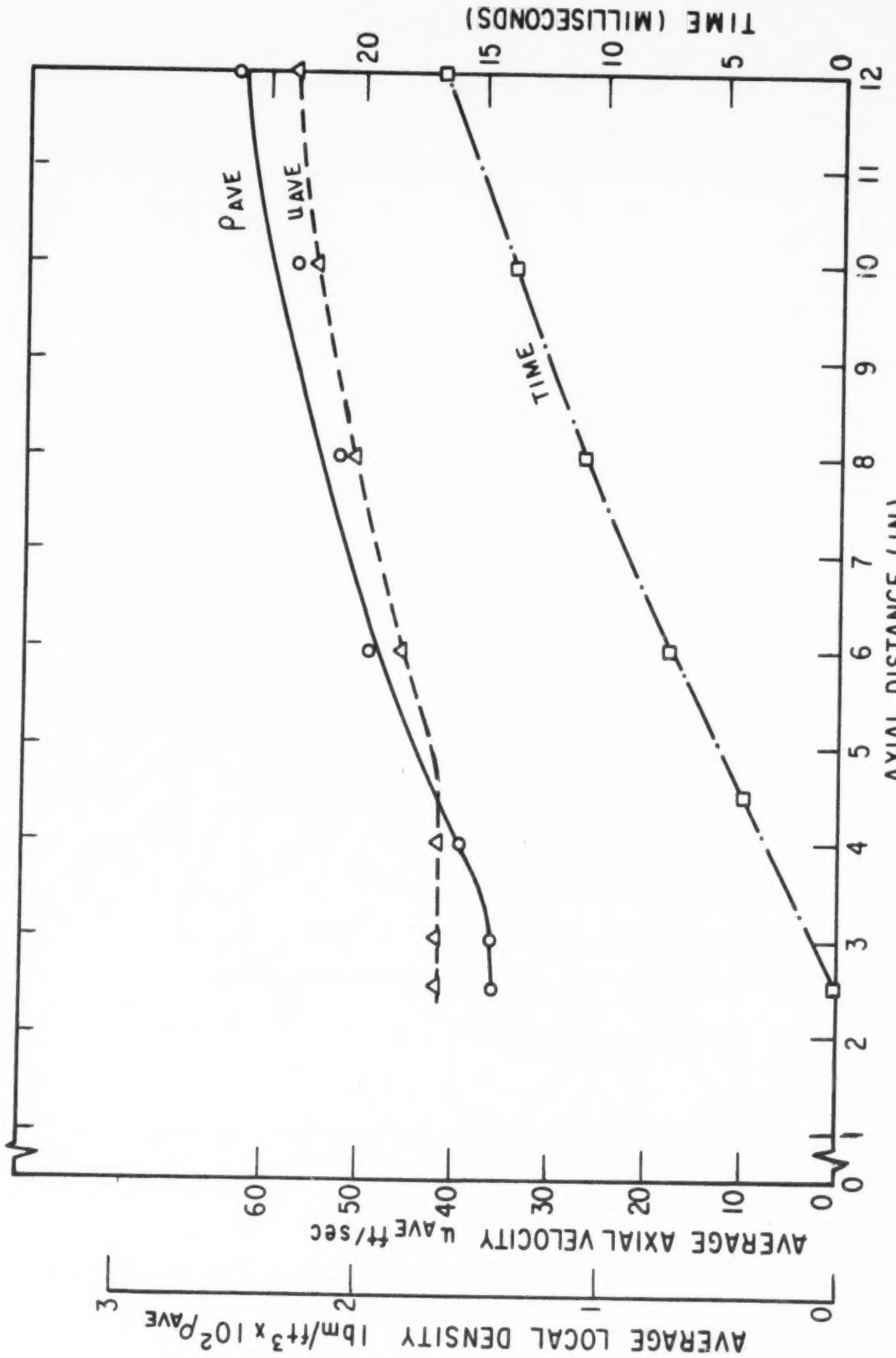

Figure 38. Axial Distribution of Averaged Density and Velocity (Calculated From Measured Temperatures) - $\Phi_o = 0.27$, L.V.N.

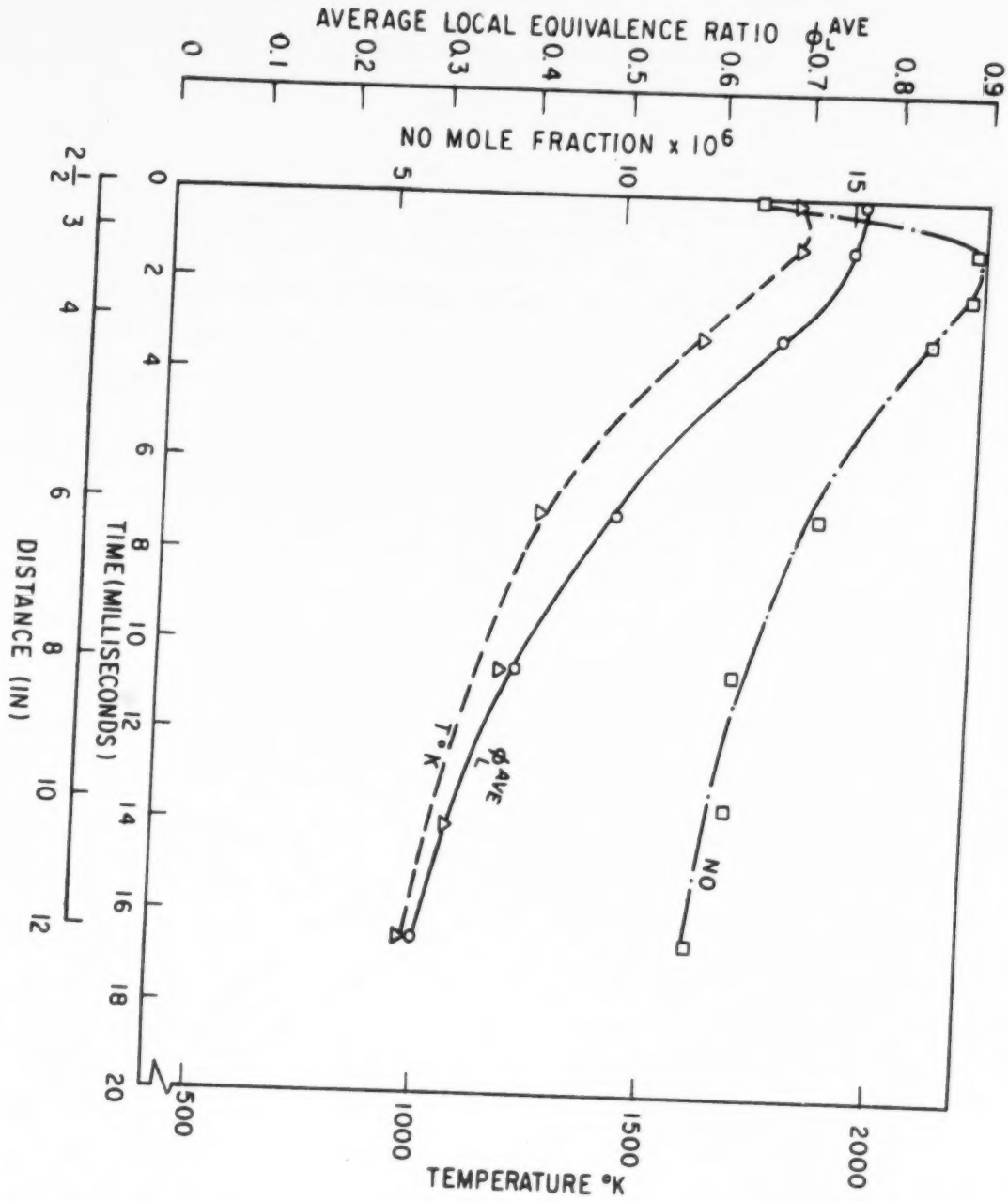

Figure 39. Time Histories of Averaged Local Equivalence Ratio, Temperature and NO Concentrations - φ_o = 0.27, L.V.N.

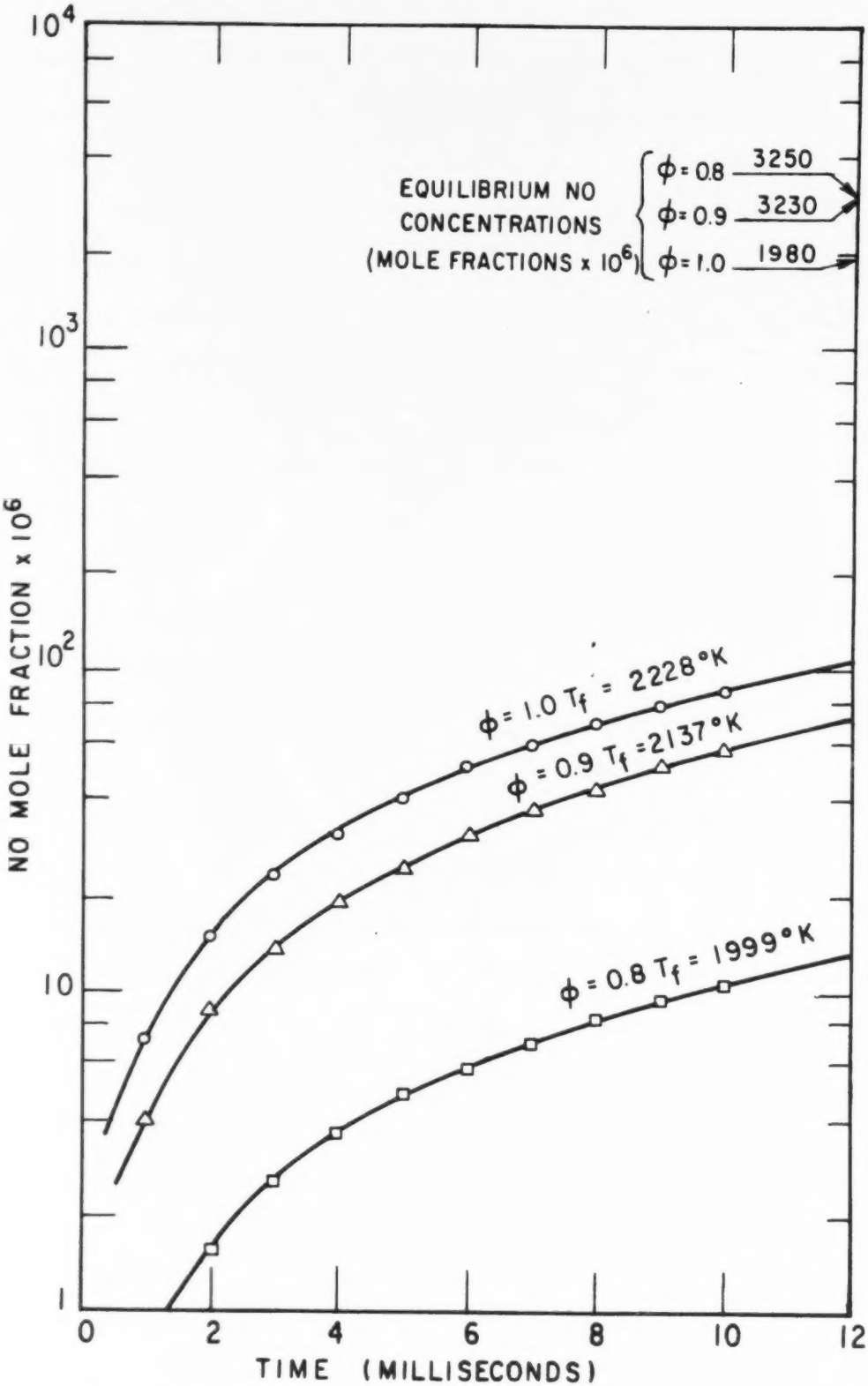

Figure 40. Non-Equilibrium NO Formation in the Products of Adiabatic Combustion of Methane and Air - $T_{initial} = 298^{o}K$, p = 1 ata

In order to compare this residence time in high temperature zone with the characteristic time of NO formation process under similar circumstances, an analytical study of the kinetics of NO formation was performed using the Zel'dovich mechanism (Appendix C). In Fig. 40, the NO mole fraction is plotted as a function of time for several equivalence ratios in adiabatic methane - air combustion assuming the temperature of the products of combustion to remain fixed at adiabatic flame temperature during NO formation. It is seen that the time required for attainment of equilibrium NO concentration would be significantly larger than the residence time estimated above. Hence, one may conclude that the production of NO in the primary zone is rate limited and that the residence time in the high temperature zone is not sufficient for equilibrium concentration of NO to be attained.

The factors which govern the rate of formation of NO in hydrocarbon - air combustion are temperature, equivalence ratio and pressure. The effect of temperature on the local concentrations of NO is seen in Figs. 27 and 28 and $2\frac{1}{2}$" and 3" stations respectively, where high temperatures ($\sim$ 2000°K) necessary for NO formation exist. The radial profiles of temperatures corrected for radiation loss of thermocouple correspond well with the NO concentration profiles in agreement with kinetic prediction. Incidentally, a comparison of these profiles in the latter part of the combustor (Figs. 33, 34) shows that the regions of high temperature are still coincident with regions of high NO concentrations, leading to the conclusion that individual fluid elements tend to preserve their identity till their exit from the combustor.

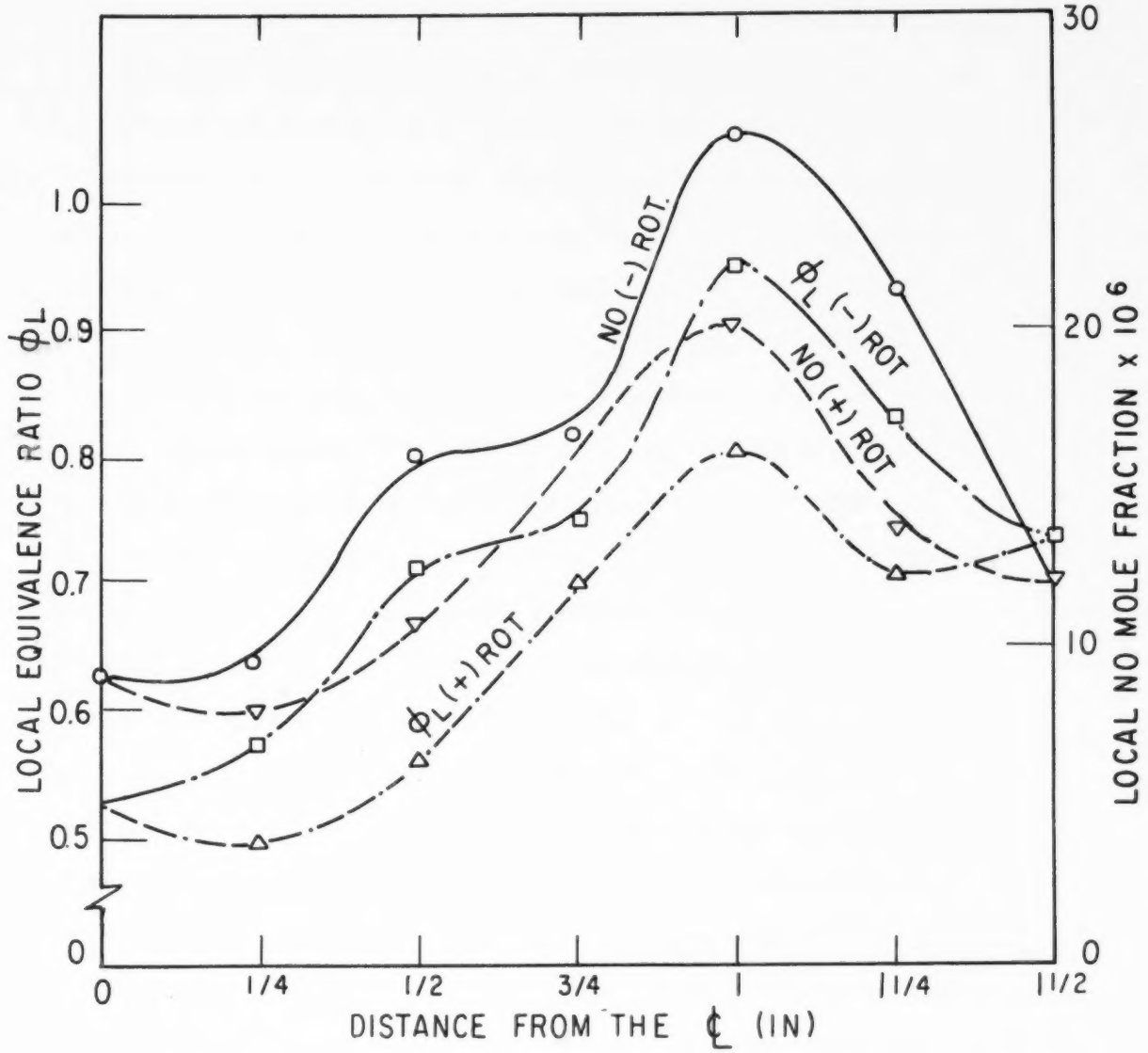

Figure 41. Radial Distributions of NO and Local Equivalence Ratio at 3" Axial Station - φ_o = 0.27, L.V.N.

The effect of local equivalence ratio on the local NO concentrations is seen in Fig. 41. This is the only case where the samples were analyzed for all the five species (CO, CO_2, O_2, unburned HC's and NO) concurrently. It is seen that high local equivalence ratios are accompanied by high local NO concentrations. This observation is in agreement with an analytical prediction arrived at by an examination of Figs. 37 and 40. As seen from Fig. 37, the maximum equilibrium NO concentration occurs in adiabatic methane - air combustion at $\varphi = 0.84$ where an optimum compromise is obtained between availability of O_2 and high adiabatic flame temperature. However, when only a limited time is available for NO formation, the temperature effect overshadows the O_2 availability requirement and the rate limited NO concentrations in stoichiometric combustion are higher than those found in off stoichiometric combustion (Fig. 40). Hence, regions of stoichiometric combustion in the primary zone are the seat of production of high concentrations of NO.

Due to the above effect, a gaseous fuel is obviously at an advantage compared to a liquid fuel as far as emissions of NO are concerned. As remarked earlier, the primary zone of a combustor using liquid fuel injection is characterized by locally fuel rich combustion regions. This results in high local temperatures in the primary zone accompanied by high local NO concentrations. The combustion of a gaseous fuel, on the other hand, can take place at substantially leaner local equivalence ratios leading to local temperatures and NO concentrations significantly lower than those for liquid fuel. This observation is supported by a comparison of the results of this experiment with those obtained previously with heptane [18]. For

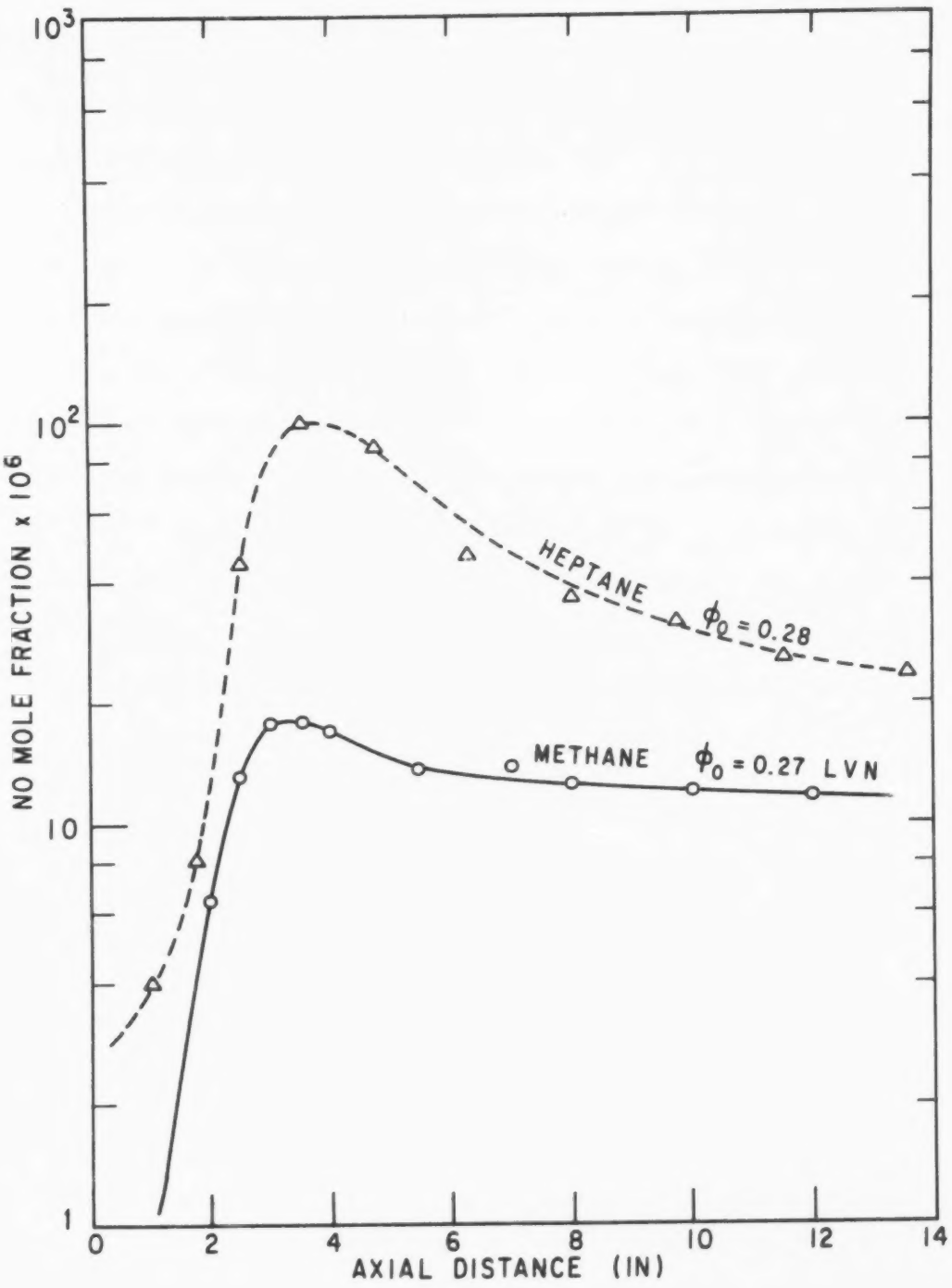

Figure 42. Comparison of Averaged Axial NO Distribution for Methane and Heptane

comparable fuel flow rates and overall equivalence ratios, the NO concentrations in the case of methane were found to be significantly lower than those for heptane (Fig. 42).

Since mixing time in droplet burning dominates the reaction time, while the mixing time is considerably smaller than reaction time for a gaseous fuel, it is possible to exercise better control of local equivalence ratio in the primary zone while using gaseous injection. This observation is substantiated by the success of prevaporizing technique in gas turbine combustors for smoke abatement [31] which also requires a careful control of the local equivalence ratios. This suggests that prevaporization of a liquid fuel before its injection can afford better control of local equivalence ratio in the primary zone and hence would lead to reduced NO emissions from gas turbine combustors.

4. CONCLUSIONS

(1) Comparison of the estimate of the characteristic time of combustion flow processes with characteristic time for NO formation indicates the production of NO in primary zone to be rate controlled. No evidence of the decomposition of NO was found.

(2) The local equivalence ratios in the primary zone strongly influence emission levels of CO and NO. Lean local equivalence ratios in the primary zone reduce both CO and NO. Regions of stoichiometric combustion are seat of production of high NO concentrations.

(3) Better control of local equivalence ratios in the primary zone may be obtained by use of gaseous fuel or by prevaporization of a liquid fuel before injection leading to reduced level of NO emissions.

(4) Knowledge of axial distribution of averaged local equivalence ratios leads to an estimation of airflow distribution in the combustor. The latter is affected both by the total airflow rate and heat release rate in the primary zone.

(5) Influence of the overall equivalence ratio on hydrocarbon and CO emissions was confirmed as originally obtained in [18]. Quenching of oxidation reactions in the latter part of the secondary zone was identified as being responsible for increased hydrocarbons and CO emissions with decreasing overall equivalence ratio.

(6) The low velocity nozzle gives a centralized fuel distribution while the high velocity nozzle leads to a rapid mixing and hence has a poor weak extinction performance.

(7) Thermocouple measured temperatures in the combustor when corrected for radiation loss, approached the adiabatic flame temperatures corresponding to local equivalence ratios.

(8) The general success of the gas sampling technique for studying the generation of air pollutants in gas turbine combustion was demonstrated by this work. The acquisition of meaningful data for NO requires gas sampling at greater number of locations compared to that needed for other species investigated.

REFERENCES

1. Control Techniques for Carbon Monoxide, Nitrogen Oxides and Hydrocarbon Emissions from Mobile Sources, U.S. Dept. of H.E.W., N.A.P.C.A., March 1970.

2. Cornelius, Stivender, Sullivan, "A Combustion System for a Vehicular Regenerative Gas Turbine Featuring Low Air Pollutant Emissions," SAE Transactions, vol. 76 (1967), paper 670936.

3. Korth, Rose, "Emissions from a Gas Turbine Automobile," SAE paper 680402, presented at mid-year meeting, Detroit, May 1968.

4. Starkman, E. S., "Fundamental Processes in Nitric Oxide and Carbon Monoxide Production from Combustion Engines," presented at May 1968 FISITA Meeting, Barcelona, Spain, Proceedings Paper No. 2-21.

5. Starkman, E. S., "Theory, Experiment and Rationale in the Generation of Pollutants by Combustion," 12th Symposium on Combustion, The Combustion Institute, Pittsburgh, Pa., 1969.

6. Newhall, H. K., "Kinetics of Engine Generated Nitrogen Oxides and Carbon Monoxide," 12th Symposium on Combustion, The Combustion Institute, Pittsburgh, Pa., 1969.

7. Caretto, Sawyer, Starkman, "Formation of Nitric Oxide in Combustion Processes," College of Engineering Rept. No. TS-68-1, March 1968, Univ. of Calif., Berkeley.

8. Obert, E. F., "Internal Combustion Engines," Third Edition, 1968 International Textbook Co.

9. Durrant, Fiorello, Faitani, et. al., "Combustor Design Changes Reduce Smoke from Gas Turbine Engines," SAE Journal June 1969.

10. Fiorello, S. C., "The Navy's Smoke Abatement Program," SAE Paper 680345.

11. Faitani, J. J., "Smoke Reduction in Jet Engines Through Burner Design," SAE Paper No. 680348.

12. Lozano, Melvin, Hochheisen," Air Pollution Emissions from Jet Engines," Journal of Air Pollution Control Association, June 1968.

13. George, Verssen, Chass, "Jet Aircraft: A Growing Air Pollution Source," Journal of Air Pollution Control Association, November 1969.

14. Northern Research and Engineering Corporation," Nature and Control of Aircraft Engine Exhaust Emissions," Rept. No. 1134-1, November 1968.

15. Smith, Sawyer, Starkman, "Oxides of Nitrogen from Gas Turbines," Journal of Air Pollution Control Association, January 1968.

16. Lieberman, A., "Composition of Exhaust from a Regenerative Gas Turbine System," Journal of Air Pollution Control Association, March 1968.

17. George, R. E., and Burlin, R. M., "Air Pollution from Commercial Aircraft in Los Angeles County," Los Angeles County Air Pollution Control District, April 1960.

18. Sawyer, Teixeira, Starkman, "Air Pollution Characteristics of Gas Turbine Engines," College of Engineering Rept. No. TS-69-1, Univ. of Calif., Berkeley.

19. Sawyer, Starkman, "Gas Turbine Exhaust Emissions," SAE Paper No. 680462.

20. "Air Pollution Abatement Qualities of Natural Gas as a Fuel for Internal Combustion Engines," California Air Resources Board 1969.

21. Cornelius and Wade, "The Formation and Control of Nitric Oxide in a Regenerative Gas Turbine Burner," SAE Paper 700708.

22. "Literature of Combustion of Petroleum," Advances in Chemistry, Series 20, pp. 33, Am. Chem. Soc. (1958).

23. Information Supplement, Beckman Model 400 FID Hydrocarbon Analyzer, The Beckman Instruments, Inc.

24. Paterson, McElroy, Sawyer, Singh, "A Prototype Chemiluminescent NO Analyzer," College of Engineering Report No. TS-70-9, Univ. of Calif., Berkeley

25. Singh, Sawyer, et. al., "Rapid Continuous Determination of NO in Exhaust Gases," Journal of Air Pollution Control Association, February 1968.

26. Lefebvre, A. H., "Progress and Problems in Gas Turbine Combustion," Tenth Symposium on Combustion, The Combustion Institute, Pittsburgh, Pa., 1965.

27. Graves, C. C., and Grobman, J. S., "Theoretical Analysis of Total Pressure Loss and Airflow Distribution for Tubular Turbojet Combustors with Constant Annulus and Liner Cross Sectional Areas," NACA Report No. 1373, 1958.

28. Marteney, Pierre J., "Analytical Study of the Kinetics of Formation of Nitrogen Oxide in Hydrocarbon-Air Combustion," Combustion Science and Technology 1970, vol. 1, pp. 461-469.

29. Final Results of the 1970 Intercollegiate Clean Air Car Race Released from the Office of Public Relations, Massachusetts Institute of Technology, Cambridge, Massachusetts, Sept. 1970.

30. Fristrom and Westenberg, "Flame Structure," McGraw-Hill Book Co., 1965, pp. 151.

31. Maybach, G. W., "The Film Vaporization Principle for Gas Turbine Combustors," Final Report, Contract No. NONR 656(13), Dept. of Mechanical Engineering, Pennsylvania State University, March 1956.

APPENDIX A

Conversions for Emission Data

Most of the gas analysis instrumentation gives a reading of the mol fraction of a particular species in a gas sample. For the purpose of setting emission standards, however, it is more convenient to relate the mass of pollutants emitted to the mass of fuel burned. The measure used presently for emission of pollutants from motor vehicles is gms of pollutant emitted per mile of vehicle travel. The conversion relations between various measures are derived as follows:

Let Y_{ppm} = mol fraction of species Y in parts per million

N_y = mol fraction of species Y

$$= \frac{\text{moles of Y in exhaust}}{\text{Total no. of moles in exhaust}}$$

$\hat{M}_y$ = molecular weight of species Y

$\hat{M}_{exh}$ = average molecular wt. of exhaust

$\dot{m}_a$ = mass flow rate of air

$\dot{m}_f$ = mass flow rate of fuel

φ = equivalence ratio

$$= (A/F)_s / (A/F)_{actual}$$

$(A/F)_s$ = stoichiometric air/fuel ratio

$(A/F)_{actual}$ = actual air/fuel ratio

EI_y = emission index of species Y

$$\triangleq \frac{\text{mass of Y}}{\text{mass of fuel}} \times 10^3$$

Now,

$$Y_{ppm} = N_y \times 10^6 = \frac{\text{moles of Y in exhaust}}{\text{total no. of moles in exhaust}} \times 10^6$$

$$= \frac{\text{mass of Y}}{\hat{M}_y} \cdot \frac{\hat{M}_{exh}}{\text{mass of exhaust}} \times 10^6$$

mass of exhaust = mass of fuel + mass of air

$$= \dot{m}_f + \dot{m}_a$$

$$= \dot{m}_f \left[1 + \frac{\dot{m}_a}{\dot{m}_f}\right]$$

$$= \dot{m}_f \left[1 + \frac{(A/F)_s}{\varphi}\right]$$

$$Y_{ppm} = \frac{\hat{M}_{exh}}{\hat{M}_y} \cdot \left(\frac{\dot{m}_y}{\dot{m}_f}\right) \frac{10^6}{\left[1 + \frac{(A/F)_s}{\varphi}\right]}$$

$$= \frac{\hat{M}_{exh}}{\hat{M}y} \cdot (EI_y) \frac{10^3}{\left[1 + \frac{(A/F)_s}{\varphi}\right]}$$

$$\therefore \boxed{(EI_y) = \frac{\hat{M}y}{\hat{M}_{exh}} \left[1 + \frac{(A/F)_s}{\varphi}\right] Y_{ppm} \times 10^{-3}} \qquad (1)$$

To obtain gms of Y/mile it is necessary to know m_f/mile for the vehicle averaged over the H.E.W. 7 cycle emission test.

Let F_M = Mass of fuel consumed (average) per mile (gms/mile).

Then $EI_y \triangleq \frac{\dot{m}_y}{\dot{m}_f} \times 10^3$

$$\boxed{Y_m = F_m \times (EI_y) \times 10^{-3} \text{ gms/mile}} \qquad (2)$$

where Y_m = gms of Y emitted/mile.

APPENDIX B

Calculation of Local Equivalence Ratio

Consider the incomplete combustion reaction of methane assuming a local equivalence ratio of φ.

Then

$$\varphi\ CH_4 + (2O_2 + 2 \times 3.77N_2) \rightarrow \nu_1\ CO_2 + \nu_2\ CO + \nu_3\ CH_4 + \nu_4\ H_2O + \nu_5\ O_2 + \nu_6\ N_2$$

NO is not considered since its concentration is very low (< 100 ppm)

The atom conservation equations are:

$$C : \nu_1 + \nu_2 + \nu_3 = \varphi \quad (1)$$

$$H : 4\nu_3 + 2\nu_4 = 4\varphi \quad (2)$$

$$O : 2\nu_1 + \nu_2 + \nu_4 + 2\nu_5 = 4 \quad (3)$$

$$N : 2\nu_6 = 2 \times 2 \times 3.77 \quad (4)$$

Thus we have four equations for the seven unknowns $\nu_1 \ldots \nu_6$ and φ. To determine these seven unknowns we require three additional independent relations. These are provided by the measured mole fractions of CO_2, CO and CH_4 in dry exhaust gas. These are:

$$N_{CO_2} = \frac{\nu_1}{\Sigma\nu_i - \nu_4} \quad (5) \qquad ; \quad N_{CO} = \frac{\nu_2}{\Sigma\nu_i - \nu_4} \quad (6) \qquad ; \quad N_{CH_4} = \frac{\nu_3}{\Sigma\nu_i - \nu_4} \quad (7)$$

From (2),

$$\nu_4 = 2(\varphi - \nu_3) \quad (8)$$

Substituting (8) in (3) we get

$$\nu_5 = 2 - \nu_1 - \frac{\nu_2}{2} - \varphi + \nu_3 \quad (9)$$

Substituting for φ in (9) from Eq. (1),

$$\nu_5 = 2 - 2\nu_1 - \frac{3\nu_2}{2} \tag{10}$$

$$\therefore \Sigma\nu_i - \nu_4 = \nu_1 + \nu_2 + \nu_3 + \nu_5 + \nu_6$$

$$= 2 - \nu_1 - \frac{\nu_2}{2} + \nu_3 + \nu_6 \tag{11}$$

$$= 9.54 - \nu_1 - \frac{\nu_2}{2} + \nu_3$$

Substituting (11) in (5), (6) and (7),

$$\nu_1 = N_{CO_2}\left[9.54 - \nu_1 - \frac{\nu_2}{2} + \nu_3\right] \tag{12}$$

$$\nu_2 = N_{CO}\left[9.54 - \nu_1 - \frac{\nu_2}{2} + \nu_3\right] \tag{13}$$

$$\nu_3 = N_{CH_4}\left[9.54 - \nu_1 - \frac{\nu_2}{2} + \nu_3\right] \tag{14}$$

$$\therefore \frac{\nu_1}{\nu_2} = \frac{N_{CO_2}}{N_{CO}}$$

$$\frac{\nu_2}{\nu_3} = \frac{N_{CO}}{N_{CH_4}}$$

$$\frac{\nu_3}{\nu_1} = \frac{N_{CH_4}}{N_{CO_2}}$$

$$\therefore \nu_2 = \frac{N_{CO}}{N_{CO_2}}\nu_1 \; ; \; \nu_3 = \frac{N_{CH_4}}{N_{CO_2}}\nu_1 \tag{15}$$

Substitute (15) in (12)

$$\therefore \nu_1 = N_{CO_2}\left[9.54 - \nu_1 - \frac{N_{CO}}{N_{CO_2}} \cdot \frac{\nu_1}{2} + \frac{N_{CH_4}}{N_{CO_2}}\nu_1\right]$$

$$= N_{CO_2}\left[9.54 - \nu_1\left\{1 + \frac{N_{CO}}{2N_{CO_2}} - \frac{N_{CH_4}}{N_{CO_2}}\right\}\right]$$

$$\therefore \nu_1\left[1 + N_{CO_2}\left\{1 + \frac{N_{CO}}{2N_{CO_2}} - \frac{N_{CH_4}}{N_{CO_2}}\right\}\right] = 9.54\ N_{CO_2}$$

$$\therefore \nu_1 = \frac{9.54\ N_{CO_2}}{\left[1 + N_{CO_2}\left\{1 + \frac{N_{CO}}{2N_{CO_2}} - \frac{N_{CH_4}}{N_{CO_2}}\right\}\right]} \qquad (16)$$

$$= \frac{9.54\ N_{CO_2}}{\left[1 + N_{CO_2} + \frac{N_{CO}}{2} - N_{CH_4}\right]} \qquad (17)$$

Similarly

$$\nu_1 = \frac{N_{CO_2}}{N_{CO}}\nu_2\ ;\ \nu_3 = \frac{N_{CH_4}}{N_{CO}}\nu_2$$

Substituting these relations into (13),

$$\nu_2 = N_{CO}\left[9.54 - \frac{N_{CO_2}}{N_{CO}}\nu_2 - \frac{\nu_2}{2} + \frac{N_{CH_4}}{N_{CO}}\nu_2\right]$$

$$= N_{CO}\left[9.54 - \nu_2\left\{\frac{N_{CO_2}}{N_{CO}} + \frac{1}{2} - \frac{N_{CH_4}}{N_{CO}}\right\}\right]$$

$$\therefore \nu_2\left[1 + N_{CO}\left\{\frac{N_{CO_2}}{N_{CO}} + \frac{1}{2} - \frac{N_{CH_4}}{N_{CO}}\right\}\right] = N_{CO} \times 9.54$$

$$\therefore \nu_2 = \frac{9.54\ CO}{\left[1 + N_{CO_2} + \frac{N_{CO}}{2} - N_{CH_4}\right]} \qquad (18)$$

Also, $$\nu_1 = \frac{N_{CO_2}}{N_{CH_4}}\nu_3\ ;\ \nu_2 = \frac{N_{CO}}{N_{CH_4}}\nu_3$$

Substituting into (14)

$$\nu_3 = N_{CH_4}\left[9.54 - \nu_3\left\{\frac{N_{CO_2}}{N_{CH_4}} + \frac{N_{CO}}{2N_{CH_4}} - 1\right\}\right]$$

$$\therefore \nu_3 = \frac{9.54\ N_{CH_4}}{\left[1 + N_{CO_2} + \frac{N_{CO}}{2} - N_{CH_4}\right]} \tag{19}$$

$$\varphi = \nu_1 + \nu_2 + \nu_3 = \frac{9.54(N_{CO_2} + N_{CO} + N_{CH_4})}{\left[1 + N_{CO_2} + \frac{N_{CO}}{2} - N_{CH_4}\right]} \tag{20}$$

Now, from (10)

$$\nu_5 = 2 - 2\nu_1 - \frac{3\nu_2}{2}$$

$$= 2 - 2x \frac{9.54\ N_{CO_2}}{\left(1 + N_{CO_2} + \frac{N_{CO}}{2} - N_{CH_4}\right)} - \frac{3}{2} \frac{9.54\ N_{CO}}{\left(1 + N_{CO_2} + \frac{N_{CO}}{2} - N_{CH_4}\right)}$$

$$= 2 - \frac{9.54}{\left(1 + N_{CO_2} + \frac{N_{CO}}{2} - N_{CH_4}\right)} \left\{2\ N_{CO_2} + \frac{3}{2}\ N_{CO}\right\}$$

$$= 2 - \nu_1\left(2 + \frac{3}{2}\frac{N_{CO}}{N_{CO_2}}\right)$$

Also,

$$\Sigma\ \nu_i - \nu_4 = 9.54\left\{1 - \frac{\left(N_{CO_2} + \frac{N_{CO}}{2} - N_{CH_4}\right)}{\left(1 + N_{CO_2} + \frac{N_{CO}}{2} - N_{CH_4}\right)}\right.$$

$$= 9.54\left\{\frac{1}{1 + N_{CO_2} + \frac{N_{CO}}{2} - N_{CH_4}}\right\}$$

$$N_{O_2} = \frac{\nu_5}{\Sigma\nu_i - \nu_4} = \frac{\left\{2 - \nu_1\left(2 + \frac{3}{2}\frac{N_{CO}}{N_{CO_2}}\right)\right\}\left(N_{CO_2} + N_{CO} + N_{CH_4}\right)}{\varphi}$$

For the reaction

$$\varphi\ CH_4 + (2O_2 + 2 \times 3.77N_2) \rightarrow \nu_1 CO_2 + \nu_2 CO + \nu_3 CH_4$$

$$+ \nu_4 H_2O + \nu_5 O_2 + \nu_6 N_2$$

N_y = mol fraction of species y in dry exhaust

Summary

$$\nu_1 = \frac{9.54\ N_{CO_2}}{\left[1 + N_{CO_2} + \frac{N_{CO}}{2} - N_{CH_4}\right]}$$

$$\varphi = \frac{9.54\left(N_{CO_2} + N_{CO} + N_{CH_4}\right)}{\left[1 + N_{CO_2} + \frac{N_{CO}}{2} - N_{CH_4}\right]}$$

$$\nu_5 = 2 - \nu_1\left(2 + \frac{3}{2}\frac{N_{CO}}{N_{CO_2}}\right)$$

$$\nu_5 = 2 - \nu_1\left(2 + \frac{3}{2}\frac{N_{CO}}{N_{CO_2}}\right)$$

$$\Sigma\nu_i - \nu_4 = \frac{9.54}{\left[1 + N_{CO_2} + \frac{N_{CO}}{2} - N_{CH_4}\right]} = \frac{\nu_1}{N_{CO_2}}$$

$$N_{O_2} = \frac{\nu_5}{\Sigma\nu_i - \nu_4}$$

$$N_{CH_4} = 6\ N_{C_6H_{14}} = 6\ N_{H/C}$$

APPENDIX C

Kinetics of NO Formation

The Zel'dovich mechanism for NO formation in high temperature air is given by the atom exchange reactions (using rate constants from Ref. 28).

$$(1)\quad N_2 + O \underset{1b}{\overset{1f}{\rightleftarrows}} NO + N$$

$$(2)\quad O + NO \underset{2b}{\overset{2f}{\rightleftarrows}} O_2 + N$$

$$k_{1f} = 6 \times 10^{13} \cdot \exp\left[-\frac{38000}{T}\right] \text{cm}^3 - \text{mole}^{-1} - \text{sec}^{-1}$$

$$k_{1b} = 3.1 \times 10^{13} \cdot \exp\left[-\frac{168}{T}\right] \text{cm}^3 - \text{mole}^{-1} - \text{sec}^{-1}$$

$$k_{2f} = 1.55 \times 10^{9} \cdot T \cdot \exp\left[-\frac{19,500}{T}\right] \text{cm}^3 - \text{mole}^{-1} - \text{sec}^{-1}$$

$$k_{2b} = 6.43 \times 10^{9} \cdot \exp\left[-\frac{3150}{T}\right] \text{cm}^3 - \text{mole}^{-1} - \text{sec}^{-1}$$

Previous studies of the kinetics of NO formation in the combustion of hydrocarbons have revealed that the reactions involving NO are considerably slower compared to the energy releasing combustion reactions. It is a good approximation, therefore, to assume that NO formation does not start until the energy releasing reactions of the C-H-O system have attained equilibrium. Further, since the equilibrium concentrations of NO are found to be less than 1/2% by volume, it is reasonable to assume that the products of combustion remain at the adiabatic flame temperature and the molecular and atomic oxygen concentrations remain fixed at their final equilibrium value. The validity of these assumptions is substantiated by the results obtained from a detailed consideration of kinetics in Ref. (28).

From Eqs. (1) and (2), the NO and N formation rates are given as

$$\frac{d[NO]}{dt} = k_{1f}[N_2][O] - k_{1b}[NO][N] + k_{2b}[O_2][N] - k_{2f}[O][NO]$$

$$\frac{d[N]}{dt} = k_{1f}[N_2][O] - k_{1b}[NO][N] + k_{2f}[O][NO] - k_{2b}[N][O_2]$$

Neglecting the contribution from $k_{1b}[NO][N]$ term at initial times due to low concentrations of both NO and N, we obtain

$$(3) \quad \frac{d[NO]}{dt} = \gamma + \alpha[N] - \beta[NO]$$

$$(4) \quad \frac{d[N]}{dt} = \gamma - \alpha[N] + \beta[NO]$$

where

$$\alpha = k_{2b}[O_2]$$

$$\beta = k_{2f}[O]$$

and $$\gamma = k_{1f}[N_2][O].$$

Differentiating (3) with respect to t,

$$(5) \quad \frac{d^2[NO]}{dt^2} = \alpha \frac{d[N]}{dt} - \beta \frac{d[NO]}{dt}$$

Adding (3) and (4) we have

$$\frac{d[NO]}{dt} + \frac{d[N]}{dt} = 2\gamma$$

$$(6) \quad \therefore \frac{d[N]}{dt} = -\frac{d[NO]}{dt} + 2\gamma$$

Substituting (6) in (5),

$$\frac{d^2[NO]}{dt^2} = \alpha\left[-\frac{d[NO]}{dt} + 2\gamma\right] - \beta \frac{d[NO]}{dt}$$

$$(7) \quad \text{i.e.} \quad \frac{d^2[NO]}{dt^2} + (\alpha + \beta)\frac{d[NO]}{dt} - 2\alpha\gamma = 0$$

The general solution of this second order linear ordinary differential equation is found to be

$$(8) \quad [NO] = \frac{2\alpha\gamma}{(\alpha+\beta)}\, t + Be^{-(\alpha+\beta)t} + A$$

where A and B are arbitrary constants to be determined from the initial conditions

$$(9) \quad [NO]_{t=0} = 0$$

$$\left.\frac{d[NO]}{dt}\right|_{t=0} = \gamma \quad \text{(From Eq. (3)}$$

Applying (9) to (8) we obtain

$$(10) \quad [NO] = \frac{2\alpha\gamma}{(\alpha+\beta)}\, t - \frac{\gamma(\alpha-\beta)}{(\alpha+\beta)^2}\left[1 - e^{-(\alpha+\beta)t}\right]$$

Calculations of [NO] as a function of time are carried out for three equivalence ratios. During the NO formation, the temperature of the products of combustion is assumed to remain fixed at the adiabatic flame temperature corresponding to a given equivalence ratio. The values of N_2, O_2 and O concentrations obtained in the equilibrium program are used for determination of the constants α, β and γ for each equivalence ratio. The pertinent data are presented in the following table [X_y = mol fraction of species Y]

MOL FRACTIONS OF N_2, O_2 AND O IN EQUILIBRIUM PRODUCTS OF ADIABATIC METHANE - AIR COMBUSTION

φ	X_{N_2}	X_{O_2}	X_O	T_f °K
1.0	0 7005	4 62x10^{-3}	2 2x10^{-4}	2228
0.9	0 7101	1 839x10^{-2}	2 4x10^{-4}	2137
0.8	0 718	3 696x10^{-2}	1 3x10^{-4}	1999

$T_{initial}$ = 298°K, p = 1 ata

The conversion from mol fractions to molal concentrations is accomplished by use of relation

$$[Y] = \frac{p}{\hat{R}T} \cdot X_y \quad \frac{\text{moles}}{\text{c.c.}}$$

where p = total pressure of the mixture $\left(\frac{Kg_f}{cm^2}\right)$

$\hat{R}$ = universal gas constant $\left(\frac{Kg_f - cm}{mol \quad °K}\right)$

T = mixture temperature (°K)

and X_y = mol fraction of species Y.

The results of the calculations are presented in Fig. 40 where the mol fraction of NO is plotted as a function of time in the initial period of NO formation for various equivalence ratios in the products of adiabatic methane - air combustion.